Influence of Ocean Alkalinity Enhancement with Olivine or Steel Slag on a Coastal Plankton Community in Tasmania

Jiaying A. Guo[1,2], Robert F. Strzepek[2], Kerrie M. Swadling[1,2], Ashley T. Townsend[3], Lennart T. Bach[1]

[1]Institute for Marine and Antarctic Studies, University of Tasmania, Hobart, Tasmania, 7000 Australia

[2]Australian Antarctic Program Partnership (AAPP), Institute for Marine and Antarctic Studies, University of Tasmania, Hobart, Tasmania, 7000 Australia

[3]Central Science Laboratory, University of Tasmania, Sandy Bay, Tasmania, 7005 Australia

Correspondence to: Jiaying A. Guo (Jiaying.guo@utas.edu.au)

Abstract. Ocean alkalinity enhancement (OAE) aims to increase atmospheric CO_2 sequestration in the oceans through the acceleration of chemical rock weathering. This could be achieved by grinding rocks containing alkaline minerals and adding the rock powder to the surface ocean where it dissolves and chemically locks CO_2 in seawater as bicarbonate. However, CO_2 sequestration during dissolution coincides with the release of potentially bio-active chemicals and may induce side effects. Here, we used 53 L microcosms to test how coastal plankton communities from Tasmania respond to OAE with olivine (mainly Mg_2SiO_4) or steel slag (mainly CaO and $Ca(OH)_2$) as alkalinity sources. Three microcosms were left unperturbed and served as a control, three were enriched with olivine powder (1.9 g L^{-1}), and three with steel slag powder (0.038 g L^{-1}). Olivine and steel slag powders were of similar grain size, but the amount of added olivine needed to be much higher than the steel slag because less alkalinity is released by the olivine than the steel slag over the 3-week experiment. Phytoplankton and zooplankton community responses as well as some biogeochemical parameters were monitored for 21 days. Olivine and steel slag additions increased total alkalinity by 29 µmol kg^{-1} and 361 µmol kg^{-1} respectively, which corresponds to a theoretical increase of 0.9 % and 14.8 % of the seawater storage capacity for atmospheric CO_2. Olivine and steel slag released silicate nutrients into the water column, but steel slag released considerably more and also significant amounts of phosphate. After 21 days, no significant difference was found in dissolved iron concentrations (>100 nmol L^{-1}) in the treatments and the control. Both minerals released dissolved aluminium (>50 nmol L^{-1}). The slag addition increased dissolved manganese concentrations (771 nmol L^{-1}), while olivine increased dissolved nickel concentrations (37 nmol L^{-1}). The slag treatment increased the total particulate manganese concentrations (22 nmol L^{-1}), while olivine increased the total particulate nickel (5 nmol L^{-1}), which was consistent with the increase in the dissolved concentrations of these trace metals in seawater. There was no significant difference in total chlorophyll *a* concentrations between the treatments and the control, likely due to nitrogen limitation of the phytoplankton community. However, flow cytometry results indicated an increase in the cellular abundance of several smaller (~<20 µm) phytoplankton groups in the olivine treatment compared to the slag treatment and the control. The abundance of larger phytoplankton (~>20 µm) decreased much more in the control than in the mineral addition treatments after day 10. Furthermore, the maximum quantum yields of photosystem II (F_v/F_m) were higher in slag and olivine treatments, suggesting that mineral additions increased photosynthetic performance. The zooplankton community composition was also affected with the most notable changes being observed in the dinoflagellate *Noctiluca scintillans* and the appendicularian

37   *Oikopleura* sp. Overall, steel slag is much more efficient for CO_2 removal with OAE than olivine and appears to induce

38   less change in the plankton community when relating the CO_2 removal potential to the level of environmental impact that

39   was observed here.

40

1 Introduction

42   Keeping global warming below 2 °C requires immediate emissions reduction. Additionally, between 450-1100 Gigatonnes

43   of carbon dioxide (CO_2) need to be removed from the atmosphere by 2100 (Smith et al., 2023). This could be achieved

44   with a portfolio of terrestrial and marine Carbon Dioxide Removal (CDR) methods. Ocean alkalinity enhancement (OAE)

45   is a marine CDR method that could theoretically contribute significantly to the global CDR portfolio (Ilyina et al., 2013;

46   Feng et al., 2017; Lenton et al., 2018).

47

48   Alkalinity is generated naturally when rock weathers and it has control on the ocean's chemical capacity to store CO_2

49   (Schuiling and Krijgsman, 2006). Natural rock weathering is currently responsible for about 0.5 Gt of atmospheric CO_2

50   sequestration every year (Renforth and Henderson, 2017). The idea behind OAE is to accelerate natural rock weathering

51   by extracting calcium- or magnesium-rich rocks, such as olivine, pulverizing them, and spreading them onto the sea surface

52   to increase chemical weathering rates (Hartmann et al., 2013). The weathering (i.e., dissolution) of these alkaline minerals

53   will consume protons (H^+), which shifts the carbonate chemistry equilibrium in seawater from CO_2 towards increasing

54   bicarbonate (HCO_3^-) and carbonate ion (CO_3^{2-}) concentrations:

55

56    $$CO_2 + H_2O \rightleftharpoons H_2CO_3 \rightleftharpoons HCO_3^- + H^+ \rightleftharpoons CO_3^{2-} + 2H^+ \tag{1}$$
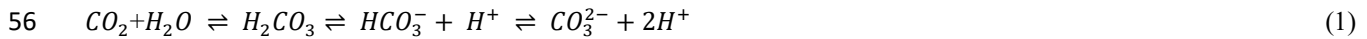
57

58   thereby making new space for atmospheric CO_2 to be dissolved in seawater and permanently stored. Previous model studies

59   have shown that OAE can mitigate climate change significantly by increasing the oceanic uptake of CO_2 from the

60   atmosphere (Kohler et al., 2010; Paquay and Zeebe, 2013; Keller et al., 2014; Lenton et al., 2018). For example, the study

61   by Burt et al. (2021) suggested that the total global mean dissolved inorganic carbon (DIC) inventories would increase by

62   156 GtC after total alkalinity is enhanced at a rate of 0.25 Pmol year^{-1} in 75-year simulations.

63

64   There are a variety of alkaline minerals that could be used for OAE. A widely considered naturally occurring mineral is

65   forsterite, a (Mg_2SiO_4)-rich olivine. This type of olivine is abundant in ultramafic rock such as dunite, constituting at least

66   88 % of the rock composition (Ackerman et al., 2009; Su et al., 2016). Olivine occurs in the Earth's crust but is more

67   abundant in the upper mantle. There are at least several billion tons of olivine resources on Earth (Caserini et al., 2022).

68   However, the extraction of olivine in 2017 was only around 8.4 Mt year^{-1} (Reichl et al., 2018), which is about two orders

69   of magnitude below the mass needed for climate-relevant OAE with olivine (Caserini et al., 2022). The net reaction for

70   CO_2 sequestration with Mg_2SiO_4 is:

71

72    $$Mg_2SiO_4 + 4CO_2 + 4H_2O \rightarrow 2Mg^{2+} + 4HCO_3^- + H_4SiO_4 \tag{2}$$

73

74   Another potential OAE source material is steel slag (Renforth, 2019), a by-product of steel manufacturing. During steel

manufacturing, high-purity calcium oxide (CaO) is used to improve the quality of the steel through accumulation of unwanted materials such as sulphur and phosphorus. Steel slag mainly contains CaO, SiO_2, Al_2O_3, Fe_2O_3, MgO, and MnO (Kourounis et al., 2007), and the chemical composition can vary depending on the manufacturing process (Wang et al., 2011). Due to the presence of CaO and potentially other alkaline components, steel slag can increase alkalinity when dissolved in seawater. The chemical reaction for CO_2 sequestration with CaO is:
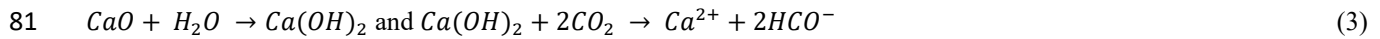
$$CaO + H_2O \rightarrow Ca(OH)_2 \text{ and } Ca(OH)_2 + 2CO_2 \rightarrow Ca^{2+} + 2HCO^- \tag{3}$$

Some of the steel slag that is produced during steel manufacturing is further used (e.g., for road construction and civil engineering) but in some countries like China, 70.5 % of steel slag is left unused and stored in dumps (Guo et al., 2018). In 2016, more than 300 million tons of steel slag was not used effectively, thereby occupying the land and raising environmental concerns (Guo et al., 2018). The effective alkaline composition, availability, and relatively low cost of the raw materials make olivine and steel slag potential source materials for OAE.

To assess whether OAE is viable, it needs to be understood how its application may affect marine biota such as plankton and the biogeochemical fluxes they drive. Some data on the effects of OAE with sodium hydroxide (NaOH) on plankton communities have recently been published (Ferderer et al., 2022; Subhas et al., 2022), but to the best of our knowledge, no such data are available for olivine- and/or slag-based OAE. Chemical perturbations via olivine and slag should be like those by NaOH in that they increase seawater pH and shift the carbonate chemistry equilibrium (see Eq. 1). However, there would be additional chemical perturbations because minerals contain a variety of potentially bioactive elements that are released into the environment when they dissolve in seawater (Bach et al., 2019). One particular concern is that natural and anthropogenic minerals such as olivine and steel slag are rich in bioactive metals that are usually scarce in the ocean, such as iron (Fe), copper (Cu), nickel (Ni), manganese (Mn), zinc (Zn), cadmium (Cd), and chromium (Cr). Many of these trace metals are essential micronutrients for phytoplankton growth (Sunda, 2000; Sunda, 2012), such as being co-factors for various metalloenzymes (summarized by Twining and Baines, 2013). It is possible that the addition of alkaline minerals may benefit phytoplankton by providing trace metals currently limiting phytoplankton growth (Falkowski, 1994; Basu and Mackey, 2018). For instance, the addition of Fe is well known to stimulate phytoplankton blooms in those vast ocean regions where Fe levels limit growth (Boyd et al., 2007; Moore et al., 2013). However, some trace metals can also inhibit phytoplankton growth, and different phytoplankton species have different requirements and tolerances for trace metals (Sunda, 2012) so the addition of trace metals via OAE may change phytoplankton community composition.

Here, we describe a microcosm experiment with coastal Tasmanian plankton communities that was used to investigate: (1) how effectively OAE via the application of finely ground olivine and steel slag could sequester atmospheric CO_2, and (2) if /how olivine and steel slag additions affect various components of the plankton community.

2 Methodology

2.1 Microcosm setup
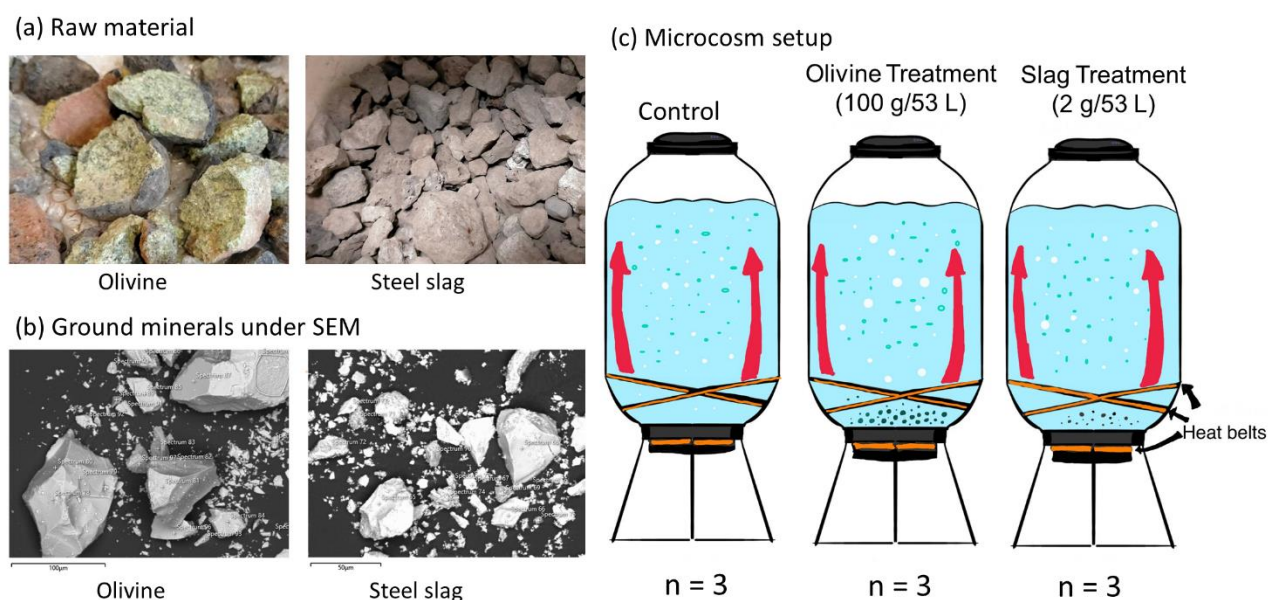
Fig. 1. Experimental design and alkalinity sources. (a) Raw materials used as alkalinity sources: olivine (left) and steel slag (right). Olivine and steel slag were originally larger than 20 mm. (b) Ground minerals observed with a scanning electron microscope (SEM). (c) Microcosm setup: each microcosm enclosed ~ 53 L of surface seawater with natural plankton communities. Olivine and steel slag treatments and the control were kept in a temperature-controlled room and two heat belts were attached to the bottom of each microcosm to create convective circulation.

We used nine 53 L transparent Kegland® Fermzilla conical unitank fermenters (polyethylene terephthalate) (Fig. 1) as microcosms to incubate natural plankton communities. All microcosms were prewashed with hydrochloric acid (10 % v/v) and rinsed five times with 18.2 MΩ Milli-Q water. Seawater with coastal plankton communities was collected at Battery Point, Tasmania (42.892°S, 147.337°E) within 2 hours by lowering the microcosms into the ocean with a crane and filling them in a manner similar to a Niskin bottle, as described in detail in Ferderer et al. (2022). A sieve with a mesh size of 2 mm was attached to the top and bottom of the microcosms during filling to avoid the entrapment of large and patchily distributed organisms in the microcosms. The enclosed seawater weight was initially between 52.35-54.70 kg. After seawater collection, filled microcosms were immediately transported back to the Institute for Marine and Antarctic Studies (University of Tasmania) on a truck and transferred within 75 min into a temperature-controlled room set to 7.5-8 °C. Two heat belts were attached to the bottom of each microcosm to induce a convective mixing current (Ferderer et al., 2022). Seawater temperature inside the microcosms was about 13.5 °C due to the heating effects of the heat belts and was the same as the sampled region. LED light strips were used to provide an average light intensity of 236 µmol photons m^{-2} s^{-1} (ranging from 208 to 267 µmol photons m^{-2} s^{-1}) with a daily light-dark cycle of 10:14 hours. The light intensity was the average light intensity in each microcosm measured with a LICOR light meter at 0.15 m depth within the microcosm. Microcosms positioned in the temperature-controlled room were shuffled anti-clockwise every day to ensure similar light

134 intensity for each microcosm throughout the experiment. Treatments were established 24 hours after collecting the seawater.

135 The total alkalinity released per amount of mineral powder added was much higher for the slag powder than the olivine

136 powder in our preliminary test trials. So, three microcosms were enriched with 100 g of olivine powder, three microcosms

137 with 2 g of steel slag powder, while the remaining three microcosms were left unperturbed and served as controls.

138

139

140 **2.2 Preparation of olivine and steel slag powder**

141 The olivine rocks were provided by Moyne Shire Council who sourced the mineral from a quarry in Mortlake, Victoria,

142 Australia. The Basic Oxygen Slag (hereafter referred to as "slag") was provided by Bradley Mansell who sourced the

143 material from Liberty Primary Steel Whyalla Steelworks in Whyalla, South Australia, Australia. Upon delivery, the olivine

144 rocks were 40-80 mm in diameter, and slag aggregates were 20-50 mm in diameter. These were crushed to smaller than 10

145 mm pieces using a hydraulic crusher. The crushed material was further ground with a ring mill with a chrome milling pot.

146 Afterwards, finely-ground samples were sieved to get samples with 150 ~ 250 µm grain size. The sieved olivine and slag

147 grains were inspected for their appearance and elemental composition using a Hitachi SU-70 analytical field emission

148 scanning electron microscope (SEM), and energy dispersive spectrometers (Central Science Laboratory (CSL), University

149 of Tasmania). Grain size spectra were determined with a Sympatec QICPIC particle size analyser LIXCELL (CSL,

150 University of Tasmania).

151

152 **2.3 Seawater sampling**

153 Seawater was transferred with a peristaltic pump from the microcosms at a depth of about 0.15 m into 1 L acid-washed

154 sampling bottles (LDPE) using an acid-washed silicon tube. Seawater in these bottles was then subsampled for dissolved

155 trace metal samples, filtrations, Fast Repetition Rate fluorometry (FRRf), and flow cytometry analysis. Samples for

156 nutrients and total alkalinity (TA) were transferred using the same pump but through a silicone tube into 80 mL HDPE

157 bottles. Total alkalinity and macronutrient samples were filtered during this process through a 0.2 µm nylon filter attached

158 to the silicone tube to remove all particles and organisms > 0.2 µm.

159

160 **2.4 Salinity, nutrients, carbonate chemistry, and trace metal analysis**

161 Salinity was measured before and at the end of the experiment using a HACH HQ40d portable meter. The pH_T (total scale)

162 and temperatures were measured daily (2-3 hours after the onset of the light period) using a pH meter (914

163 pH/Conductometer Metrohm). We recorded voltages and temperature from the pH meter and calibrated the pH_T at original

164 temperature at sampled time using the certified reference material (CRM) Tris buffer following the method described in

165 SOP6a by Dickson et al. (2007). Briefly, the standard buffer's pH and voltage at different temperature gradients were

166 recorded, and temperature vs. voltage polynomial regression data were generated for calculating calibrated pH values (pH_T)

167 (refer to Eq. 3 in SOP6a of Dickson et al. (2007)). The regression could then be used to obtain a CRM pH value for each

168 temperature and to calibrate the pH measured in the microcosms to the total pH scale.

169

170 Total alkalinity was sampled every four days. It was measured in duplicate using a Metrohm 862 Compact Titrosampler
171 coupled with an Aquatrode Plus with PT1000 temperature sensor following the SOP3b open-cell titration protocol
172 described in Dickson et al. (2007). Filtered TA samples were stored at 8 ℃ for a maximum of 23 days before measurement.
173 Titration curves were evaluated using the "calkulate" script within PyCO2sys by Humphreys et al. (2022). The carbon
174 chemistry equilibrium was calculated with the R package "seacarb" Gattuso et al. (2023) from pH_T, TA, phosphate, silicate,
175 temperature, and salinities using stoichiometric equilibrium constants from Lueker et al. (2000). Dissolved macronutrients
176 were measured every second day using standard spectrophotometric methods developed by Hansen and Koroleff (1999)
177 on the day the samples were taken from the microcosms.

178

179 Dissolved trace metal concentrations were measured four times during the experiment: a few hours before olivine and slag
180 were added, a few hours after these minerals were added on day 2, near the middle of the experiment on day 13, and at the
181 end of the experiment on day 22. Sixty mL of seawater was collected using an acid-washed 60 mL syringe, and the seawater
182 was filtered through 25 mm diameter 0.2 µm pore size polycarbonate filters. Unfortunately, we did not notice that 0.2 µm
183 pore size nylon filters (acid washed) were used during sampling on days 1 and 2 so we refiltered these seawater samples
184 again using 0.2 µm pore size polycarbonate filters after one month. All seawater samples were diluted approximately 20-
185 fold by weight using Milli-Q water (18.2 MΩ·cm grade) and acidified using 1 % ultrapure HCl. These samples were
186 analysed using Sector Field Inductively Coupled Plasma Mass Spectrometry (SF-ICP-MS) employing multiple resolution
187 settings to overcome major spectral interferences. Due to the presence of abundant major metal ions in our samples, such
188 as Na and Mg, natural open-ocean seawater from the Southern Ocean with very low trace metal concentrations was diluted
189 20 times with Milli-Q water and used as a representative blank. The same Southern Ocean seawater was enriched with
190 different gradients of trace metal standards to calculate the samples' trace metal concentrations. Five of the total 36 samples
191 had abnormal trace metal concentrations, and 2 of them were from day 1. We considered values as outliers using the
192 interquartile range (IQR) criterion on pre-addition data, and if values are more than 10 times higher than replicates, they
193 are also considered as outliers. These samples containing outliers were excluded from the data analysis (Table S1.). The
194 major likely source of these metal contaminations is sampling in the temperature control room, where precautions were
195 insufficiently implemented.

196

197 **2.5 Particulate matter and plankton community analysis**

198 Chlorophyll *a* was sampled every second day by filtering the seawater through glass fibre filters (GF/F, pore size = 0.7 µm,
199 diameter =25 mm), and filters were stored in 15 mL polypropylene tubes wrapped with aluminium foil and stored at -80 ℃
200 for 50-70 days before measurement. Each filter was immersed in 10 mL 100 % methanol for 18-20 h to extract chlorophyll
201 from phytoplankton and these samples were analysed on a Turner fluorometer (Model 10-AU) following the method
202 described by Evans et al. (1987).

203

204 Phytoplankton flow cytometry samples were fixed with 40 µL of a mixture of formaldehyde-hexamine (18 %:10 % v/w)
205 added to 1400 µL of seawater sample. All bacteria samples (700 µL) were fixed with 14 µL glutaraldehyde (Electron-
206 microscope grade, 25 %). After mixing samples with fixatives, samples were stored for 25 minutes at 10 ℃, then flash-
207 frozen in liquid nitrogen, and stored at -80 ℃ until measurement 83-86 days later. Directly before the measurement,
208 samples were thawed at 37 ℃. Bacteria samples were stained with SYBR green I (diluted in dimethylsulfoxide) at a final

209   ratio of 1:10000 (SYBR Green I: sample).

210

211   A Cytek Aurora flow cytometer (Cytek Biosciences) was used to quantify the abundance of fluorescing particles such as

212   phytoplankton or stained bacteria. Phytoplankton groups were distinguished based on their fluorescence signal intensity of

213   different laser excitation/emission wavelength combinations and forward scatter (FSC). The yellow-green laser (centre

214   wavelength: 577 nm), in combination with FSC signal strength, was used to separate cyanobacteria and cryptophytes from

215   other phytoplankton. The violet laser (centre wavelength: 664 nm) in combination with FSC was used to distinguish

216   picoeukaryotes, nanoeukaryotes, and microphytoplankton. The blue laser (centre wavelength: 508 nm) in combination with

217   FSC was used to distinguish bacteria from other living (i.e., DNA-containing) particles (Fig. S. 1).

218

219   The biovolume of each classified flow cytometry phytoplankton type was calculated using the equation:

220

221    $Biovolume = Cell\ number\ count \times (\frac{FSC}{10248})^{2.14}$ (4)

222

223   where biovolume is the biovolume of the phytoplankton (μm^3), cell number is the cell count per mL of sample, and the

224   FSC is the forward scatter signal value from the flow cytometry. This equation is calculated based on the relationship

225   between biovolume and FSC for different phytoplankton species (Selfe, 2022). The biovolume of each phytoplankton type

226   was then divided by the total biovolume of all phytoplankton type to calculate the biovolume proportion of each

227   phytoplankton type (Biovolume prop.). This derived value was used to estimate the phytoplankton composition in each

228   microcosm.

229

230   Phytoplankton photosynthetic performance was estimated from the rapid light curves measured with an FRRf (FastOcean

231   Sensor FRRf3, Chelsea Instruments Group) every second day following the protocol adapted from Schallenberg et al.

232   (2020). Samples were kept in the dark for 20 minutes before the measurement and then added to the FRR fluorometry

233   cuvette, which was temperature-controlled at 13.5 °C. Filtered natural seawater was used for blank correction. A channel

234   with three light wavelengths (450, 530, and 624 nm) was used in each acquisition sequence. At least 10 acquisitions were

235   measured for each sample. The maximum electron transport rate (ETR_{max}), initial slope of the rapid light curve (α), and the

236   light-saturation parameter (E_k) were calculated using the equation described by Platt et al. (1980) without photoinhibition:

237

238    $ETR = ETR_{max} [1 - e^{-\frac{\alpha E}{ETR_{max}}}]$ (5)

239

240   These parameters together with the maximum quantum yield of PSII (F_v/F_m) were used to compare the photosynthetic

241   performance of the phytoplankton communities in different microcosms.

242

243   Seawater was sampled before the treatment and at the end of the experiment for particulate trace metal concentrations.

244   Samples of 100 mL were filtered through an acid-cleaned polycarbonate filter (25 mm diameter, 0.8 μm pore size) and

245   placed in an acid-cleaned polypropylene filter holder in a trace metal-clean laminar flow bench. The filters were washed

246   with the EDTA-oxalate reagent (1.4 mL) twice (8 min total) and rinsed with chelexed NaCl solution (0.6 mol L^{-1} with 2.38

247   mmol L^{-1} of HCO_3^-, pH=8.2) 10 times (1.5 mL aliquots) (Tovar-Sanchez et al., 2003; Tang and Morel, 2006). Filters were

248   stored in acid-washed well plates at -20 °C before analysis. The digestion process followed the method reported by Bowie

249 et al. (2010). Briefly, all samples and triplicate certified reference materials plankton standards (50 mg/vial) were digested

250 in a mixture of strong ultrapure acids (750 μL 12 mol L^{-1} HCl, 250 μL 40 % HF, 250 μL 14 mol L^{-1} HNO$_3$) in 15 mL Teflon

251 perfluoroalkoxy (PFA) vials on a 95 ℃ hot plate for 12 h in a fume hood. They were then dry evaporated for 4 h and re-

252 suspended in 10 % v-v ultrapure HNO$_3$. All prepared solutions had indium as internal standard added to a final

253 concentration of 10 μg L^{-1}. Three pre-mixed multi-element standard solutions (MISA) were prepared as external calibration

254 standards.

255

256 Particulate organic carbon (POC) was sampled by filtering 100 mL of seawater from each microcosm. Glass fibre filters

257 (Whatman GF/F, pore size =0.7 μm, diameter =13 mm) were pre-combusted at 400 ℃ for 6 h. Filters were stored at -20 ℃

258 before measurement. Samples were treated via fuming with 2N HCl to remove carbonates overnight and dried in the oven

259 for 4h. Finally, filters were folded into silver cups and stored in a desiccator until analysis. Samples were analysed for

260 carbon with a Thermo Finnigan EA 1112 Series Flash Elemental Analyser (CSL, University of Tasmania).

261

262 Biogenic silica (BSi) concentrations were analysed every 4 days by filtering 100 mL of seawater from each microcosm.

263 Mixed Cellulose Ester (MCE) membrane filters (diameter = 25 mm, pore size = 0.8 μm) were used for BSi samples. BSi

264 filters were placed in a plastic petri dish and stored at -20 ℃ before measurement. Filters were processed using the hot

265 NaOH digestion method of Nelson et al. (1989). The final solution was measured using the same process as the dissolved

266 silicate (see section 2.4).

267

268 A self-made plastic zooplankton net (20 mm height and 15 mm width) with a 210 μm mesh size was acid-washed first and

269 then used to collect zooplankton from microcosms before mineral addition on day 2, near the middle (day 13), and at the

270 end of the experiment (day 23). Samples were stored in 10 % formalin seawater solutions and kept at room temperature

271 until measurements. Zooplankton were quantified and identified under a Leica M165C microscope fitted with a Canon 5D

272 camera. The number of zooplankton from one mini-trawl in each collection was converted to the unit of individual L^{-1} and

273 used for data analysis. The diversity of zooplankton communities was estimated with the Shannon Diversity Index (H)

274 calculated as:

275

276 $H = -\sum(pi \times \ln(pi))$ (6)

277

278 where pi is the proportion of the entire zooplankton community made up of individual species abundance, and ln is the

279 natural logarithm.

280

281

282 **2.6 Statistic analysis**

283 R studio was used for data analyses. Generalized additive models (GAMs) from the package "mgcv" were fitted to the data

284 to predict the changes over time. The GAMs all shared the same equations:

285

286 $Y = s(Day),$ (7)

287

288 in which Y presents the dependent variable and s(Day) is the smooth term of the day of the experiment. Another GAM was
289 used to detect significant differences between treatments and the control:

291 $$Y = Treatment + s(Day) + s(Day, by = oTreatment) \tag{8}$$

293 In this equation, the variable "Treatment" includes three conditions: "Control", "Slag" and "Olivine"; while "oTreatment"
294 is the ordered factor of the variable "Treatment" which allowed us to compare the GAMs smooth terms from different
295 treatments and the control (Simpson, 2017).

297 When comparing GAMs, P-means represent the p-value obtained from comparing two GAMs, such as the control and the
298 olivine treatment. If P-means is below 0.05, it indicates that the mean values of the two GAMs exhibit significant
299 differences over the course of the experiment. Conversely, if P-means is equal to or greater than 0.05, it suggests that the
300 two GAMs have similar mean values. In contrast, P-smooths represents the p-value derived from comparing the smooth
301 terms of two GAMs. If P-smooths is below 0.05, it indicates that the two GAMs demonstrate significantly different trends
302 in their change over time.

304 For the analysis of trace metal concentrations and zooplankton abundance, Generalized Linear Models (GLMs) from the
305 'stats' package were fitted to the data to determine significant differences between treatments and the control. The selection
306 of specific GLMs was based on the distribution of the raw data. One GLM equation is

308 $$Y = Treatment + \frac{Day}{22} + \left(\frac{Day}{22}\right)^2 \tag{9}$$

310 with family = Gamma, where Y represents the measured parameter (abundance of a zooplankton species and dissolved
311 trace metal concentrations); treatment is the conditions ("Control", "Slag" and "Olivine"); and Day represents the day of
312 the experiment. The other GLM equation,

314 $$Y = Treatment + Day \tag{10}$$

316 with family = Gaussian, was employed for particulate trace metal data and the Shannon Diversity Index. To compare the
317 contribution of the three treatments on the measured parameters, Tukey's significant difference test was conducted on the
318 GLMs using the 'glht' function.

320 **3. Results**

321 **3.1 Elemental composition and grain size of the finely-ground minerals**

322 SEM analysis revealed the approximate elemental composition of olivine and slag powder (Table 1). Based on this analysis
323 the olivine composition resembles the Mg-rich olivine mineral "forsterite" (Mg_2SiO_4). The particle size spectrum of olivine
324 powder is shown in detail in Fig. S2. Roughly 69 % of the olivine particles, when measured by volume, fell within the

325 diameter range of 35 - 300 µm. Additionally, SEM analysis revealed high levels of Ca and O in the slag, indicative of the

326 considerable Ca(OH)$_2$ and CaO content of the powder (Table 1; please note that H cannot be measured with the applied

327 method). The particle size measurement (Fig. S2) showed that 78 % of the ground slag particles were between 35 - 300

328 µm.

329

330 **Table 1.** The weight percentage of elements from two minerals. Unit: wt %.

Element	O	Ca	Mn	Si	Mg	Fe	Al	Ti	Cr	Ni
Olivine	39.9	0.4		19.9	26.4	13.0	1.0			0.8
Steel slag	41.9	36.0	7.0	6.5	4.3	3.7	3.4	1.7	1.6	

331

332

333 **3.2 Physical and chemical conditions over the course of the experiment.**

334 On day 2 of the experiment, when olivine particles were introduced into the microcosms, the smallest fraction of the powder

335 remained suspended, causing the seawater to become highly turbid for several days. The resulting milky appearance of the

336 seawater eventually faded over a period of approximately five days, and by day 5, the turbidity had visually become like

337 the slag treatment and the control. This effect was not anticipated, and as a result, we decided to investigate its impact on

338 light intensity. To do so, a test was conducted after the main experiment in which olivine powder was added to a microcosm

339 identical to those used in the experiment, and light intensity was measured daily at a depth of 0.15 m. The results showed

340 that the addition of olivine caused an initial reduction in light intensity of 18.5 % at 15 mins after addition, which declined

341 to 7.4 %, 3.7 %, 3.7 % and 0 % after 1, 2, 3, and 4 days, respectively. These findings indicate that olivine additions can

342 significantly affect the light environment in the microcosms, whereas no such effect was observed in the slag treatment.

343
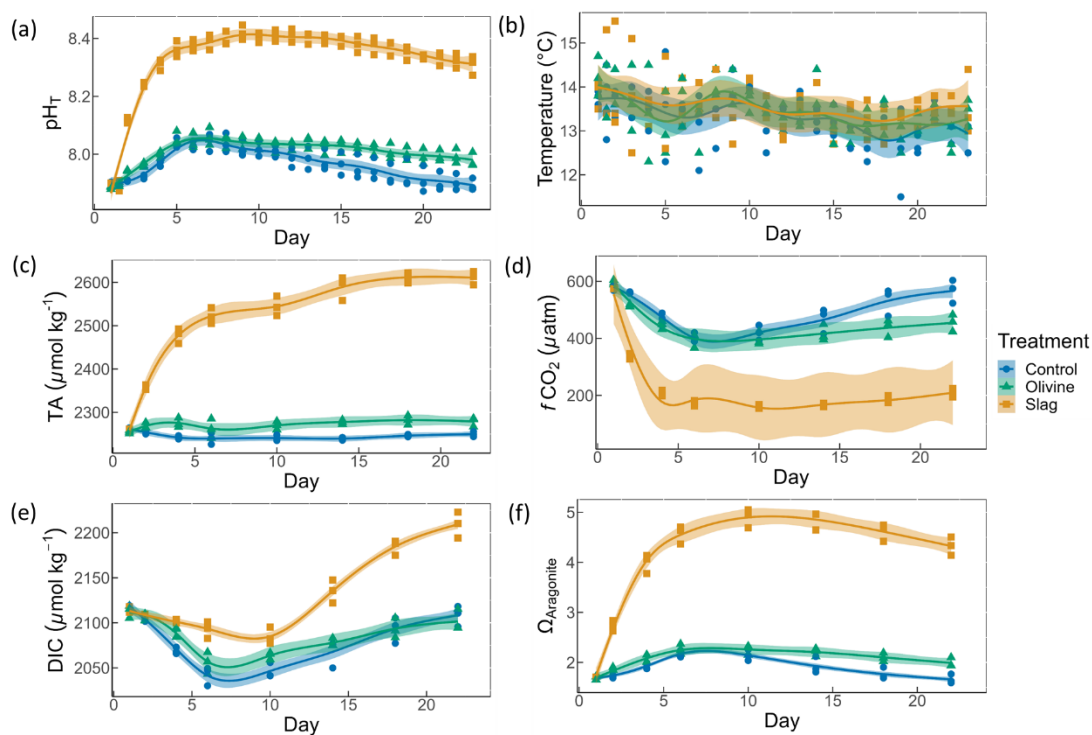
344

345 **Fig. 2**. Carbonate chemistry conditions. The temporal development of (a) pH$_T$, (b) temperature, (c) total alkalinity (TA), (d) CO$_2$ fugacity

(fCO₂) computed at *in situ* temperature and atmospheric pressure, (e) dissolved inorganic carbon (DIC), and (f) aragonite saturation state ($\Omega_{aragonite}$). The dots represent the raw data (n=3 for each treatment per sampling time), and the fitted curve is the generalized additive model (GAM). The shading represents the 95 % confidence interval of the fitted GAM.

The pH_T of all microcosms increased from day 1 to day 5 (Fig. 2a). This was due to photosynthetic CO_2 drawdown in the control or photosynthetic CO_2 drawdown in combination with alkalinity release from minerals in the treatments. During the peak of the bloom, pH_T was 8.037 ± 0.010 in the control (average values $\pm$ standard error), 8.054 ± 0.014 in the olivine treatment and 8.411 ± 0.015 in the slag treatment. The pH_T was significantly higher in the slag than the olivine treatment and the control throughout the experiment (control and olivine pH_T were not significantly different). The final pH_T of the control, olivine, and slag treatments were 7.893 ± 0.012, 7.978 ± 0.015, and 8.309 ± 0.019, respectively. The temperature inside of the microcosms varied between replicates, which may have added noise in the biological response data. However, on average there was no statistically significant difference between control/treatments during the experiment.

In our data analysis, all the fitted GAMs from the treatments and the control exhibited significant differences in pH_T from each other, as evidenced by the p-values of both P-means and P-smooths being smaller than 0.001. For detailed results of the GAM p-values, please refer to Table S2.

Total alkalinity increased marginally from 2255 ± 2 to 2262 ± 13 μmol kg⁻¹ within the first 6 days after olivine addition while it increased more substantially from 2259 ± 1 to 2522 ± 11 μmol kg⁻¹ in the same time span in the slag treatment (Fig. 2c). The TA in the control decreased from 2261 ± 2 μmol kg⁻¹ to 2240 ± 7 μmol kg⁻¹ from day 1 to day 6 but remained stable thereafter. The TA reached 2279 ± 6 μmol kg⁻¹ in the olivine treatment and 2611 ± 9 μmol kg⁻¹ in the slag treatment on day 22. The slag treatment reached a significantly higher TA than the olivine treatment and the control (P-smooths < 0.001). The mean TA from GAM in olivine treatment was higher than the control (P-means < 0.001).

The CO_2 fugacity (fCO₂) computed at *in situ* temperature and atmospheric pressure decreased continuously in the first 6 days in all microcosms (Fig. 2d). Then it increased again in the control and olivine treatments while staying lower in the slag treatment (P-means and P-smooths $\leq$ 0.001 between either treatment or the control). Dissolved inorganic carbon (Fig. 2e) and the aragonite saturation state ($\Omega_{aragonite}$; Fig. 2f) revealed a similar trend over the course of the experiment in the control and the olivine treatment. In contrast, the slag treatment had higher DIC and $\Omega_{aragonite}$ values throughout the experiment (P-means < 0.001).
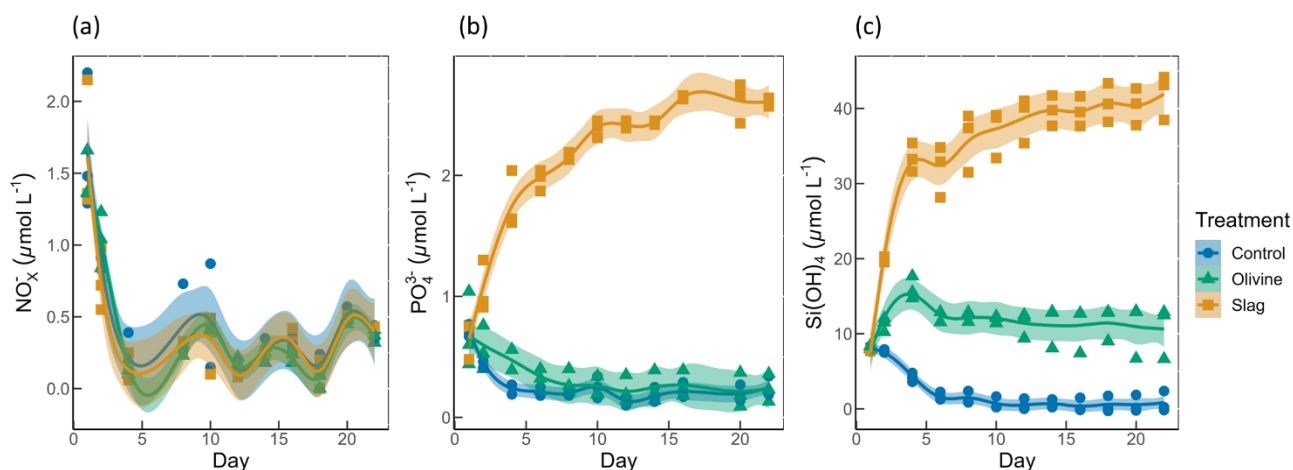
377 **Fig. 3.** Macronutrients concentrations over the course of the study. (a) Nitrate and nitrite concentrations. (b) Phosphate concentrations.
378 (c) Silicic acid concentrations. The dots represent the raw data (n=3 for each treatment per collection), and the fitted curve is the
379 generalized additive model.

380

381 Initial nitrate and nitrite (NO_x^-), phosphate (PO_4^{3-}), and silicic acid ($Si(OH)_4$) concentrations were 1.58 ± 0.12, 0.69 ± 0.59,
382 and 8.04 ± 0.10 µmol L^{-1}, respectively (Fig. 3). NO_x^- declined rapidly in all microcosms once the experiment had
383 commenced to values below 0.5 µmol L^{-1} and no significant difference was detected between treatments and control (P-
384 smooths >0.05; Fig. 3a). In both the olivine treatment and the control, the PO_4^{3-} concentration decreased in the first six
385 days (Fig. 3b). In the slag treatment, PO_4^{3-} increased to a maximum of 2.65 ± 0.01 µmol L^{-1}, which was significantly higher
386 than in the olivine treatment and the control (P-means <0.001). The $Si(OH)_4$ concentration increased to a maximum of
387 15.99 ± 0.87 µmol L^{-1} in the olivine treatment, increased to a maximum of 41.92 ± 1.75 µmol L^{-1} in the slag treatment, but
388 decreased below the detection limit in the control (Fig. 3c). Significant differences were observed in the development of
389 $Si(OH)_4$ between all treatments and the control (Table S2).

390
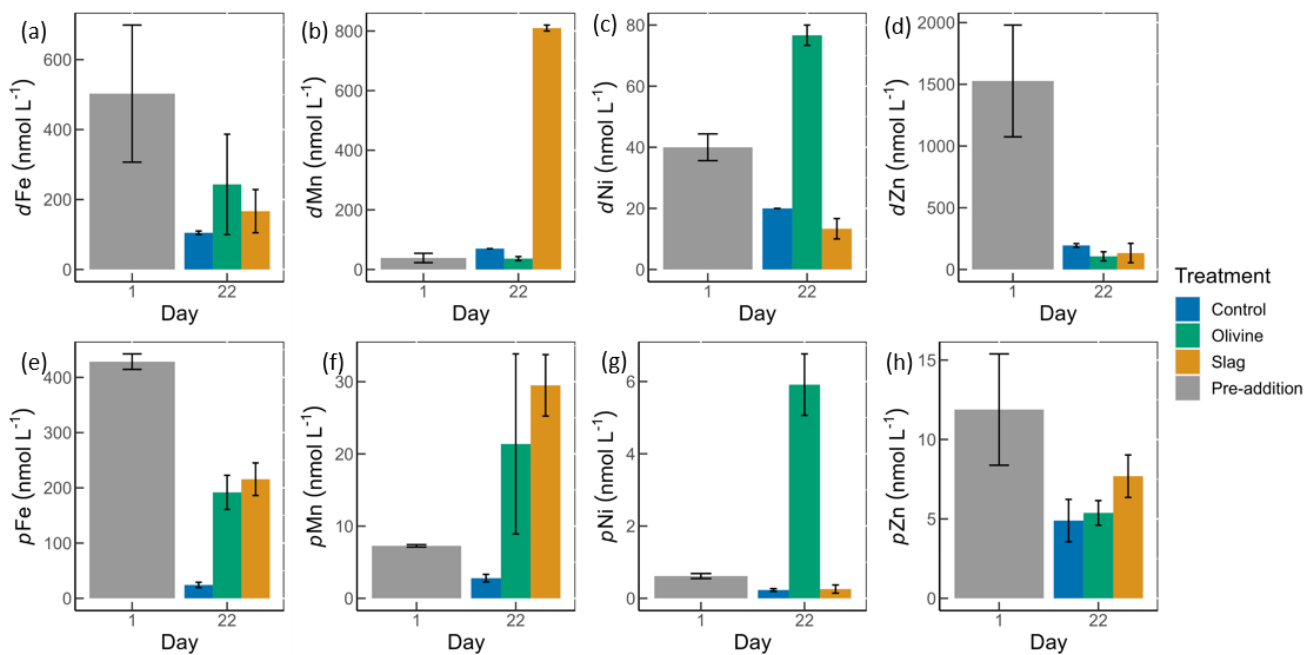
391
392

393 **Fig. 4.** Dissolved and particulate trace metal concentrations in microcosm seawater. (a)-(d) are dissolved trace metal concentrations, and
394 (e)-(h) are total particulate trace metal concentrations. The error bars represent the standard error from measured samples. The pre-
395 addition data shown in (a)-(d) represent the average of 7 microcosms before addition of slag or olivine. The data for the control on day
396 22 in (a)-(d) and for the pre-addition on day 1 in (e)-(h) were based on two of three microcosm replicates. The remaining data were based
397 on all three microcosm replicates.

398

399 The dissolved trace metal concentrations measured from microcosms are presented in Fig. S3. While the mass of olivine
400 added to the microcosms was 50-fold greater (100 g vs 2 g), it's noteworthy that the variation in dissolved trace metal
401 concentrations between the two treatments were much smaller than 50 folds. After 21 days of experiment, the treatments
402 showed an increase in dissolved Al concentrations from 920 ± 286 to 970 ± 228 nmol L^{-1} in olivine treatment, and from
403 920 ± 286 to 1093 ± 77 nmol L^{-1} in slag treatment, while in the control dissolved Al decreased to 230 ± 10 nmol L^{-1} (Fig.

404   S3). The fitted GLMs were compared, and the p-value revealed how much influence a treatment had on the dissolved metal

405   concentrations (Table S3). The results indicate that the slag and olivine additions led to significantly higher Al

406   concentrations than in the control (p-values < 0.05), but no significant difference was found between the two treatments

407   (p-value = 0.189). The Cu concentration in the olivine on day 22 was significantly higher than the slag treatment and the

408   control (p-value <0.05) (Fig. S3). The addition of olivine and slag released some dissolved Fe, but overall, the concentration

409   of Fe did not differ significantly between treatments (Fig. 4a, Table S3). The slag released a substantial amount of dissolved

410   Mn (maximum 810 ± 10 nmol L^{-1} on day 22) (Fig. 4b), leading to significantly higher concentrations than in the olivine

411   treatment and the control (p-values < 0.001). A significant amount of dissolved Ni (maximum 77 ± 3 nmol L^{-1} on day 22)

412   was released from the olivine powder (p-values <0.001) (Fig. 4c). The initial concentration of dissolved Zn in seawater

413   was much higher than on day 22 in all microcosms, and no significant difference in Zn concentrations was found between

414   the treatments and the control.

415

416   Particulate concentrations of some trace metals also differed between treatments. The total particulate Fe decreased in all

417   microcosms on day 22 comparing with the pre-addition level, but both mineral addition treatments had higher particulate

418   Fe concentrations than the control (Fig. 4e). The addition of slag elevated particulate Mn concentrations to a level higher

419   than the pre-addition and the control on day 22 (Fig. 4f), while the addition of olivine increased the particulate Ni

420   concentrations to a level higher than the slag, the control, and the pre-addition (Fig. 4g). The particulate Zn concentrations

421   in general decreased by the end of the experiment (Fig. 4h), and no significant differences were found between the

422   treatments and the control.

423

424   The POC on day 1 and day 22 from all microcosms were very similar, 10.99 ± 0.58 and 11.03 ± 0.41 µmol L^{-1} respectively

425   (Fig. S4) so the metal:POC results were consistent with the particulate trace metal results (Fig. 4 e-h). In general, the non-

426   surface metal:POC are positively correlated with the total metal:POC ratios (Fig. S5). The ratio of non-surface to total

427   particulate trace metal concentrations is summarized in Table S5. Both non-surface and total Fe concentrations decreased

428   in microcosms on day 22 compared with the pre-addition level. Iron:POC ratios were significantly higher in the treatments

429   than in the control on day 22 (p-values <0.05. Table S3), and there was no significant difference between mineral addition

430   treatments. The non-surface to total Fe:POC ratios were > 0.94 in all microcosms on both day 1 and day 22. The total and

431   non-surface Mn:POC ratio was the highest in the slag treatment. These ratios were higher than the pre-addition level and

432   the control at the end of the experiment. The total particulate Ni concentrations in the olivine treatment were significantly

433   higher than before olivine addition. The olivine treatment led to a >22-fold higher Ni:POC ratio compared to the other two

434   treatments (p-value <0.001).

435

436

437

 3.3 Development and physiology of the plankton community
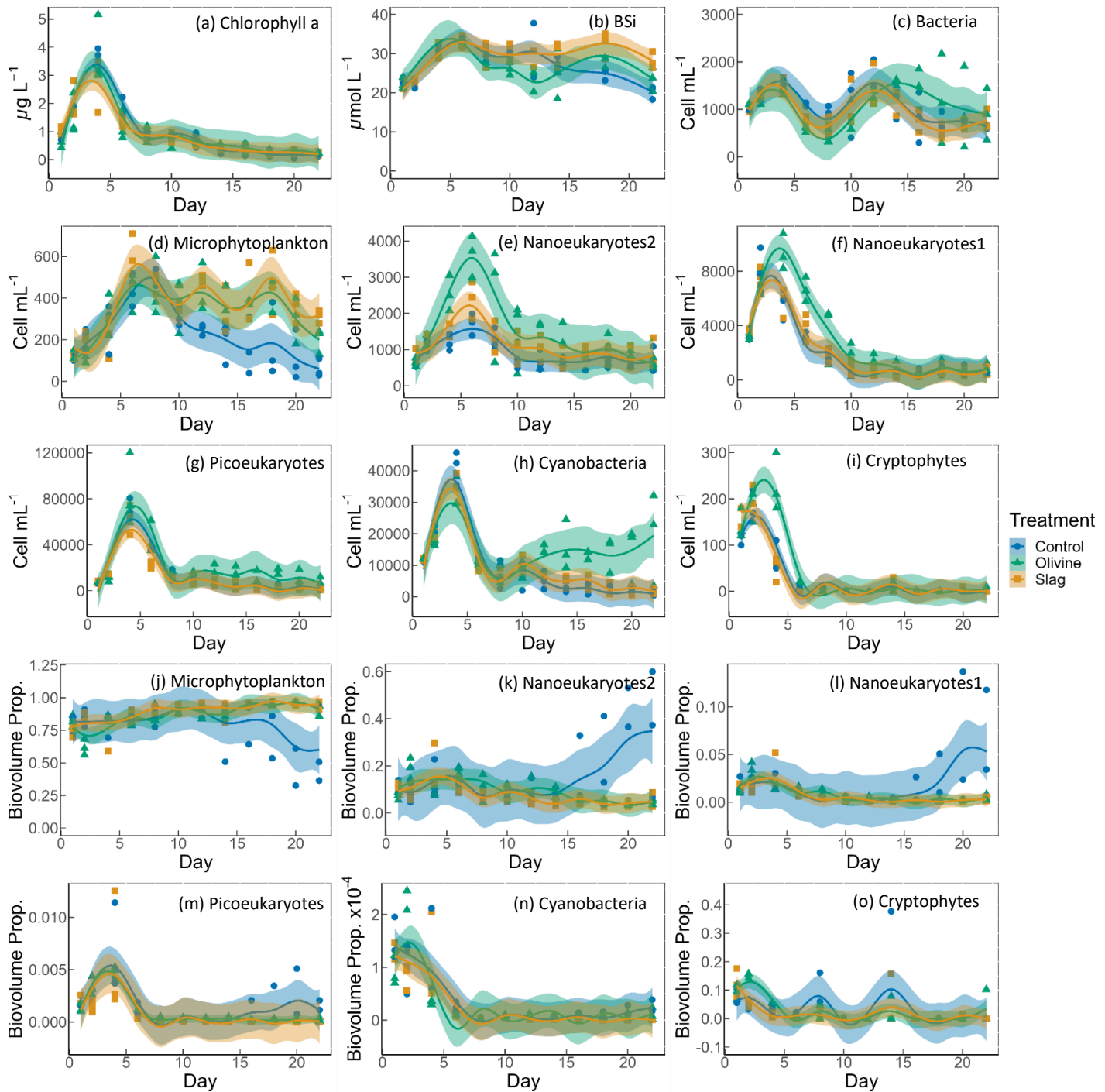
440 **Fig. 5.** Temporal development of chlorophyll a concentration (chl-a), BSi, and different eukaryotic and bacterial plankton groups as

441 determined with flow cytometry. (a) chlorophyll a; (b) BSi; cell concentrations of (c) heterotrophic bacteria, (d) microphytoplankton, (e)

442 nanoeukaryotes2, (f) nanoeukaryotes1 (g) picoeukaryotes, (h) cyanobacteria, and (i) cryptophytes; biovolume proportion of (j)

443 microphytoplankton, (k) nanoeukaryotes2, (l) nanoeukaryotes1 (m) picoeukaryotes, (n) cyanobacteria, and (o) cryptophytes. The figure

444 data points represent the raw data, and the fitted curve is the generalized additive model. The shaded area represents the 95 % confidence

445 interval.

446

447   The chl-a concentration in all microcosms increased from day 1 to day 4 from 1 µg L^{-1} to 3-4 µg L^{-1} (Fig. 5a). The chl-a

448   concentration then decreased rapidly from day 4 to day 8, then continued to decrease, though more slowly, to <0.3 µg L^{-1}

449   until the end of the experiment. The GAMs of chl-a did not show any difference between treatments and the control (both

450   P-means and P-smooths >0.05, see Table S2).

451

452   The BSi concentration increased from day 1 to day 6 in all microcosms (Fig. 5b). In the olivine treatments, BSi

453   concentrations decreased slightly after the peak until day 12 but then increased again. In the slag treatment, BSi

454   concentrations remained relatively stable after the initial phytoplankton bloom. In contrast, BSi concentration decreased

455   continuously in the control after the initial peak. Olivine particles suspended in seawater after the mineral addition (see

456   section 3.2) partially ended up on BSi filters during filtration. This led to extremely high BSi measurements on days 2 and

457   4 that were removed from Fig. 5b. Without these outliers, the mean of fitted BSi GAM in the olivine treatment was lower

458   than the control and the slag treatment (Table S2), and the slag had the highest average BSi over the course of the

459   experiment. Overall, the BSi trends in the two treatments were similar (P-smooths = 0.269), and both were significantly

460   different from the control (P-smooths <0.05).

461

462   The development of the phytoplankton community composition showed significant differences between the treatments and

463   the control. In general, most phytoplankton groups exhibited similar patterns to chl-a, with peak cell numbers occurring on

464   day 4 (Fig. 5f-i) apart from microphytoplankton and nanoeukaryotes2 which had the peak delayed for 1-2 days (Fig. 5d-

465   e). Please be aware that flow cytometers may not capture some large and chain-forming phytoplankton. After reaching

466   peak values during the bloom, phytoplankton abundance generally decreased steadily. Microphytoplankton displayed

467   similar trends to the results for BSi. Before day 10, all microcosms had similar microphytoplankton abundances (Fig. 5d).

468   However, in the control, microphytoplankton abundance declined continuously and at a faster rate compared to the two

469   treatments (P-smooths values <0.03). From day 2 to day 6, the abundance of nanoeukaryotes1, nanoeukaryotes2,

470   picoeukaryotes, and cryophytes was higher in the olivine treatment compared to the slag treatment and the control. After

471   day 8, their abundance in the olivine treatment decreased to a similar level as the slag treatment and the control. Notably,

472   there were few significant differences observed between the slag treatment and the control in terms of the abundances of

473   nanoeukaryotes1, nanoeukaryotes2, picoeukaryotes, cyanobacteria, and cryptophytes throughout the experiment. In the

474   olivine treatment, cyanobacteria experienced a second bloom after day 10, which was significantly different from the other

475   two groups (P-smooths <0.01). Heterotrophic bacteria exhibited an increase and decline pattern following the

476   phytoplankton bloom until day 8 (Fig. 5c). Subsequently, bacteria abundance increased again, reaching a second peak

477   during days 12-14, followed by a decline until the end of the experiment. The decline in bacteria abundance was slower in

478   the olivine treatment, although no significant differences were detected between treatments (Table S2).

479

480   Among all the microcosms, microphytoplankton consistently accounted for the largest proportion of biovolume. From the

481   perspective of biovolume proportion, the mineral addition mainly influenced the microphytoplankton and nanoeukaryotes.

482   The control had similar phytoplankton biovolume distribution as the treatments from day 1 to day 15, but after that the

483   proportion of microphytoplankton biovolume decreased to a level significantly lower than the treatments. In the control

484   treatment, the proportion of nanoeukaryotes' biovolume increased as the proportion of microphytoplankton decreased. The

485   biovolume of picoeukaryotes, cyanobacteria and cryptophytes increased during the phytoplankton bloom and then

486   decreased drastically after the bloom. There were no significant differences in biovolume proportion observed for

picoeukaryotes, cyanobacteria and cryptophytes between the treatments and the control.
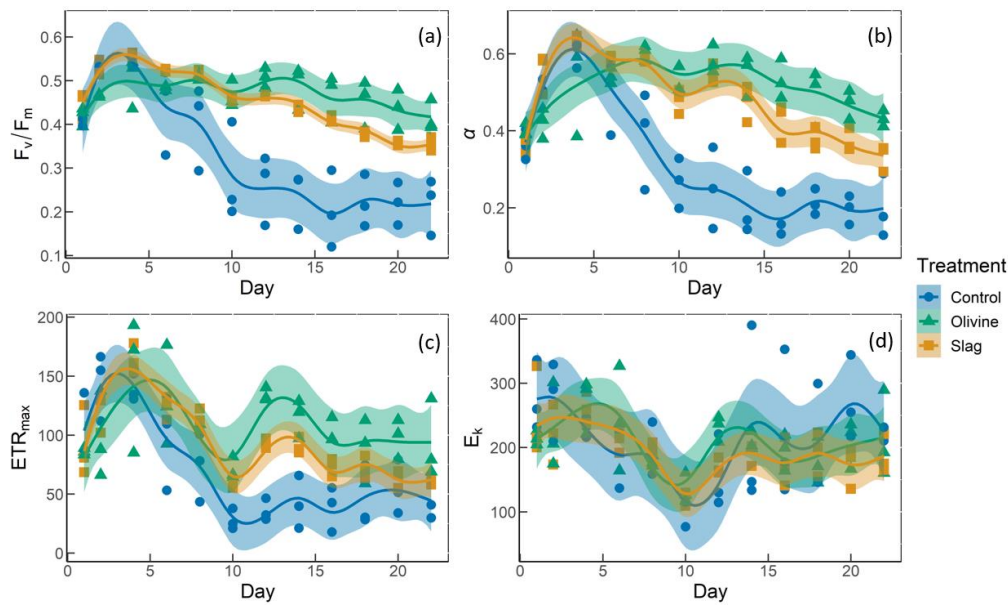
Fig. 6. The photosynthetic performance of the phytoplankton community. (a) F_v/F_m, the maximum quantum yield of photosynthesis II. (b) α, the initial slope of the rapid light curves. (c) ETR_{max} is the maximum electron transport rate, the maximum potential photosynthetic rate. (d) E_k is light-saturation parameter, Unit: μmol photons m^{-2} s^{-1}.

The temporal development of F_v/F_m, α, ETR_{max}, and E_k is illustrated in Fig. 6. The F_v/F_m values of the phytoplankton community were approximately 0.42 ± 0.01 and increased to levels > 0.5 during the peak of the phytoplankton bloom on day 4 (Fig. 6a). Following the bloom, F_v/F_m values dropped below 0.3 in the control. However, the decline in F_v/F_m after the bloom was less pronounced in the two mineral addition treatments with the olivine treatment maintaining higher F_v/F_m values than the slag treatment (P-smooths <0.05). At the end of the experiment, F_v/F_m was 0.22 ± 0.04 in the control, 0.35 ± 0.01 in the slag treatment, and 0.42 ± 0.02 in the olivine treatment. The temporal development of α aligned with the patterns observed for F_v/F_m (compare Fig. 6a and 6b). The maximum values of ETR_{max} were observed on day 4 in the control and the slag treatment, while in the olivine treatment, it occurred on day 5 (Fig. 6c). Subsequently, ETR_{max} continuously decreased until day 10 and then stabilized until the end of the experiment. However, ETR_{max} exhibited a subsequent increase in the mineral treatments around day 12. The ETR_{max} values were higher in the mineral treatments compared to the control group (P-means <0.001, Table S2). The parameter E_k decreased from 246 ± 17 μmol photons m^{-2} s^{-1} on day 1 to 121 ± 7 μmol photons m^{-2} s^{-1} on day 10, and then it increased again to approximately 200 μmol photons m^{-2} s^{-1} by the end of the experiment (Fig. 6d). The change in E_k did not exhibit significant differences between the treatments and the control (both P-means and P-smooths >0.05).
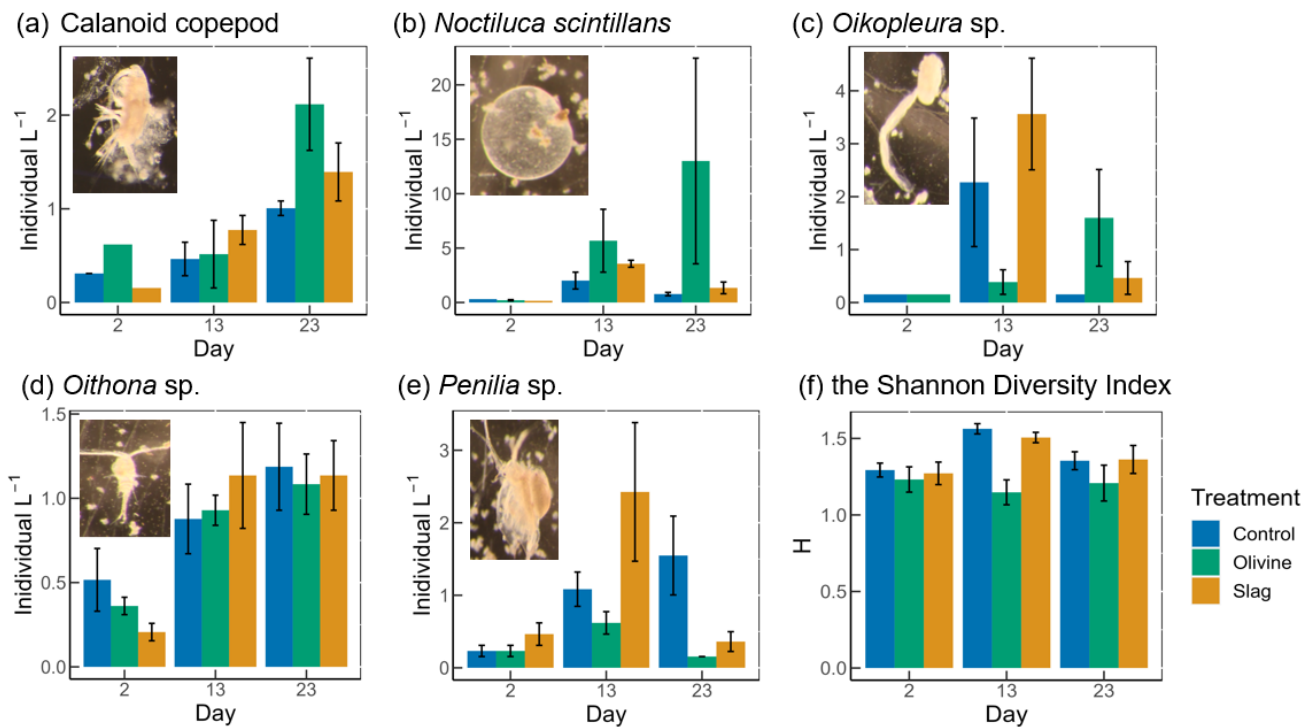
Fig. 7. The dominant zooplankton abundance and community diversity from different treatments. Abundance of dominant zooplankton in microcosms: (a) calanoid copepod; (b) *Noctiluca scintillans*; (c) *Oikopleura* sp.; (d) *Oithona* sp.; (e) *Penilia* sp.; and (f) the Shannon diversity index (H) of different treatments and the control. Error bars represent the standard error calculated from three microcosm replicates. Photographs of each zooplankton group are shown on the corresponding graphs.

Thirteen zooplankton taxonomic groups were identified in the microcosms. The dominant taxa were the appendicularian *Oikopleura* sp., the cyclopoid copepod *Oithona* sp., the cladoceran *Penilia* sp., the heterotrophic dinoflagellate *Noctiluca scintillans* and several calanoid copepods including *Acartia* sp., *Paracalanus* sp. and *Gladioferens* sp. The larvae and eggs of *Oikopleura*, *Penilia* and copepod were also observed under the microscope. In general, higher zooplankton numbers were observed after the bloom on day 13 (Fig. 7). The abundance of calanoid copepods and *Oithona* sp. increased after day 2 (Fig. 7a, d), and there was no significant difference between treatments and the control (p-values >0.05, Table S4). The abundance of *N. scintillans* increased significantly more in the olivine treatment than in the control and the slag treatment, with highest abundance of 13 ± 9 individual L⁻¹ observed in the olivine treatment on the last day (Fig. 7b). The abundance of *Oikopleura* in the control and the slag treatment was higher than the olivine treatment on day 13 but was higher in the olivine treatment on day 22 (Fig. 7c). A higher abundance of *Penilia* sp. was found in the slag treatment on day 13 and in the control on day 23 (Fig. 7e). Due to the patchy distribution of zooplankton, these data have large standard errors and only the differences in the numbers of *N. scintillans* in the olivine treatment were statistically significantly different from the slag treatment and the control (p-value <0.05, Table S4).

Considering the control and slag treatment, the Shannon Diversity Index (H) increased from day 2 to day 13 and declined on day 23, while in the olivine treatment, H was lower on day 13 than on day 2 and day 23 (Fig. 7f). The GLMs revealed that the olivine treatment had significantly lower H on day 13 than the control and the slag treatment (p-values <0.001). There were no significant differences in H between the control and the slag treatment (Table S4). The addition of olivine decreased the zooplankton community's diversity. This is mainly driven by distinct trends observed in the abundance of *Oikopleura* sp., *Penilia* sp., and *N. scintillans* (Fig. 7).

536

4. Discussion

4.1 CO_2 removal potential of slag and olivine

The slag powder created significantly higher CO_2 removal potential than the olivine powder over the course of the study. $Ca(OH)_2$ and CaO in slag and Mg_2SiO_4 in olivine are likely to be the main functional minerals driving the measured alkalinity enhancement. Total alkalinity increased by 361 $\mu mol\ kg^{-1}$ in the slag treatment while it increased by only 29 $\mu mol\ kg^{-1}$ in the olivine treatment, equivalent to a potential increase in marine inorganic carbon by 14.7 and 0.9% within 3 weeks of their application. When normalizing these alkalinity increases to the same material weight, 1 g of slag would release 9626 μmol TA while 1 g of olivine would release 16 μmol TA. Thus, over 3 weeks of experimental incubation, slag is ~600-fold more efficient in releasing alkalinity for particles of this size class (please note that particle size spectra of olivine and slag were similar but not identical; Fig. S1). We can also use these values to make a rough estimate of how much CO_2 these two minerals could potentially sequester. One mole of alkalinity from olivine and slag can sequester approximately 0.85 mole of CO_2. Thus, one tonne of slag and olivine powder as used here could sequester 360 and 0.6 kg, respectively, within 3 weeks. It is likely that optimization of particle size and application method may lead to higher efficiencies. Nevertheless, the slag showed potential as an OAE source mineral, even when applied as relatively coarse powder in this experiment.

4.2 Environmental implications of slag and olivine additions

The amount of olivine and slag powder added to the treatments differed significantly (100 g of olivine powder were added while only 2 g of slag powder were added to the 53 L microcosms). Our rationale for these different mass additions was to yield somewhat similar amounts of detectable alkalinity enhancement in the dissolved phase, since we already knew from tests before the experiment that slag elevates alkalinity faster than olivine. However, olivine was less efficient in releasing alkalinity than we had anticipated so that even a 50-fold higher addition of olivine (in mass) did not compensate for this difference. As such, our experiments are associated with an "apples and oranges issue" in that our perturbation with minerals and associated OAE differs. We argue that an adjusted addition of minerals depending on the alkalinity enhancement rate would be consistent with what OAE practitioners may do under real-world conditions. Presumably, OAE deployments may have to adjust the amounts of minerals to detect alkalinity enhancement in the dissolved phase for verification purposes. Nevertheless, to account for the "apples and oranges issue", the following discussion mainly relates the observed environmental effects with the alkalinity enhancement achieved over the course of the study.

4.2.1. OAE effects on phytoplankton physiology and community

Previous research has hypothesised that OAE-induced changes in seawater carbonate chemistry could delay phytoplankton bloom formation due to reductions in seawater pCO_2 in the aftermath of an OAE deployment (Bach et al., 2019). The build-up of chlorophyll *a* concentration as observed here was indistinguishable between treatments and the control, suggesting no effect of slag- or olivine-based OAE on phytoplankton bloom dynamics under these experimental settings. A lack of bloom delay due to carbonate chemistry is unsurprising for the olivine treatment where the release of alkalinity was small

571   (29 µmol kg^{-1} alkalinity release), but somewhat more surprising in the slag treatment where alkalinity was quite rapidly

572   increased by 361 µmol kg^{-1}. However, the release was still lower than in a very similar study by Ferderer et al., (2022)

573   where alkalinity was increased by 500 µmol kg^{-1} using sodium hydroxide and even there they did not observe a bloom

574   delay. Based on this very limited evidence, it seems that bloom delays do not occur consistently under OAE within this

575   alkalinity range.

576

577   The nutrient data show that the phytoplankton community was most likely N-limited after day 4 so that the release of

578    $Si(OH)_4$ from olivine and $Si(OH)_4$ and PO_4^{3-} from slag did not stimulate a further increase in chlorophyll-a concentration

579   in the treatments. The development of BSi concentrations is indicative of the prevalence of diatoms in the microcosms but

580   differences between treatments and the control were small. The release of $Si(OH)_4$ through olivine and slag will most likely

581   benefit diatoms but this fertilization effect did not manifest in this specific experiment because N was limiting diatom

582   growth. However, when new N is supplied then diatoms will likely take a bigger share of the limiting N pool when olivine

583   or slag are used for OAE, as has been shown in $Si(OH)_4$ manipulation experiments in and outside the context of OAE

584   research (Egge and Jacobsen, 1997; Ferderer et al., 2023). As such, diatoms are likely to benefit from olivine and slag

585   applications. In the case of slag, the release of PO_4^{3-} will likely be another driver that affects plankton productivity and

586   community composition. As for $Si(OH)_4$, however, the effect of additional PO_4^{3-} did likely not materialise in this

587   experiment because PO_4^{3-} was not limiting over the course of the study. However, in ecosystems where PO_4^{3-} is a limiting

588   resource, the application of slag could enhance productivity with associated benefits for higher trophic levels. In contrast,

589   excessive applications of slag and concomitant PO_4^{3-} release could also pose a risk of eutrophication. Future studies may

590   need to investigate what the most sustainable dose of OAE via olivine and/or slag applications could be and the suitable

591   regions for application.

592

593   The flow cytometry results further revealed the change in phytoplankton community composition. Both the olivine and

594   slag treatments sustained higher microphytoplankton abundances after the peak of the phytoplankton bloom. This trend is

595   consistent with higher F_v/F_m values in the treatments than in the control so that it is tempting to assume that

596   photophysiological fitness gain measured with the FRRf led to higher competitiveness of microphytoplankton in the

597   community. Indeed, calculations of the contribution of different phytoplankton groups to total biovolume based on flow

598   cytometry indicate that microphytoplankton were predominantly contributing to the phytoplankton community biovolume

599   so that the responses measured by the FRRf were probably to a large extent driven by this group.

600

601   Apart from the increased microphytoplankton abundance, for the slag treatment, other phytoplankton groups distinguished

602   with flow cytometry did not deviate considerably from the control. The olivine addition, however, triggered more

603   pronounced shifts in the phytoplankton community. In particular, the nanoeukaryotes (roughly between 2-20 µm),

604   picoeukaryotes and the cryptophytes showed relatively higher abundance during the peak of the phytoplankton bloom, and

605   the abundance of cyanobacteria was higher after the bloom. We speculate that this shift following olivine treatment may

606   be attributable to a top-down effect from the decrease in zooplankton grazing effects in microcosms, which will be

607   discussed in section 4.2.2.

608

609   The measurement of photophysiological parameters revealed that the phytoplankton had generally better photosynthetic

610   performance in the slag and olivine treatments than in the control, especially after the phytoplankton bloom. During the

611   first 5 days, the changes in phytoplankton photosynthetic performance were indistinguishable between the control and the

612   slag treatment, while the values of α, ETR_{max} and F_v/F_m were lower in olivine treatment. At this time all microcosms had

613   similar health because of the relatively high NO_x^- concentrations and Fe supply (around 500 nmol L^{-1}), but the suspended

614   particles in the olivine treatment may have led to artifacts in the measuring of photophysiology by FRRf. Scattering and/or

615   absorption of light by suspended olivine particles is the most parsimonious explanation for the simultaneous depression in

616   α, ETR_{max} and F_v/F_m. After day 5, the F_v/F_m, α and ETR_{max} values decreased significantly faster in the control than in the

617   treatments, and to values lower than the initial condition. A decrease of F_v/F_m is commonly associated with physiological

618   stress, such as nutrient limitation, and high light stress (Bhagooli, et al., 2021), with Fe limitation causing a more

619   pronounced decline in F_v/F_m than nitrogen limitation (Gorbunov, et al., 2021). The ETR_{max}, which represents the maximum

620   electron transport rate, has also been shown to be negatively affected when phytoplankton experience nitrogen or Fe

621   limitation (Kolber et al., 1994; Gorbunov & Falkowski 2021). Furthermore, the change in photosynthesis performance

622   after day 10 was suspected to be driven by the microphytoplankton because the decrease of F_v/F_m, α, and ETR_{max} in the

623   control was coupled with the decrease in microphytoplankton abundance while the other phytoplankton groups were in

624   low abundance as in the mineral addition treatments, and the microphytoplankton contributed significantly (75 %) to

625   community biovolume. All microcosms were similarly NO_x^- limited from day 5 onward (Fig. 3) so that N-limitation is

626   unlikely to explain different trends in photophysiological parameters between the control and OAE treatments. Trace metals,

627   especially Fe, released through slag and olivine additions could potentially explain these differences.

628

629   Several of the trace metals released from slag and olivine are required for photosynthesis. For example, Fe is required for

630   many proteins functioning in photosynthesis, such as cytochromes, ferredoxin, and superoxide dismutase (SOD) (Twining

631   and Baines, 2013), and the addition of Fe can stimulate the growth of phytoplankton (Sunda and Huntsman, 1997) and

632   increase F_v/F_m (Behrenfeld et al., 2006). The dissolved and particulate Fe concentrations were higher in mineral addition

633   treatments than in the control indicating potentially more Fe available to sustain phytoplankton photosynthesis. While this

634   explanation is intriguing for the observed trends in photophysiology, it remains unclear why such strong differences

635   occurred between mineral addition and control treatments despite dissolved Fe concentrations of ~500 nmol L^{-1} at the end

636   of the experiment in the control. In Fe-limited ocean regions, dissolved Fe is at least two orders of magnitude lower, and

637   the enhancement of Fe to ~1.5 nmol L^{-1} can induce major phytoplankton blooms and relieve photophysiological stress (De

638   Baar et al., 2005). It is possible that these coastal phytoplankton species have higher Fe requirements than those from the

639   open ocean where Fe is limiting (Strzepek and Harrison, 2004). We speculate that when Fe was consumed during the

640   phytoplankton bloom, bioavailable Fe was much lower in the control, and may have been insufficient to meet the cellular

641   requirements of coastal phytoplankton. Our findings therefore suggest that Fe perturbations is not only relevant for lower

642   Fe open ocean regions but could also be relevant for coastal ocean locations.

643

644   Alternatively, the addition of Mn, Ni and other trace metals from mineral addition may have benefited photosynthesis.

645   Manganese is required for the water-splitting reaction of photosystem II (Armstrong, 2008), and both Mn and Ni are

646   common bioactive trace metals for SODs in marine phytoplankton. The noxious superoxide anion radical (O_2^-) generated

647   from aerobic respiration and oxygenic photosynthesis could be harmful to phytoplankton physiology, and SOD removes

648   O_2^-, thus improving photosynthesis (Wafar et al., 1995; Wolfe-Simon et al., 2005). This is consistent with our

649   photosynthetic measurements. Interestingly, although the amounts and types of trace metals released from the slag and

650   olivine powders were different, they led to relatively similar F_v/F_m values with only slightly higher F_v/F_m in the olivine

than the slag treatment from days 10-21. Over this time, these trace metal additions could have fertilized different phytoplankton species (Pausch et al., 2019; Balaguer et al., 2022; Guo et al., 2022) possibly because different phytoplankton could have different trace metal requirements, such as for SOD. For example, cyanobacteria have NiSOD, diatoms have MnSOD, dinoflagellates have both FeSOD and MnSOD (Wolfe-Simon et al., 2005). Another explanation is that phytoplankton in the control were limited by bicarbonate while the treatments had sufficient bicarbonate from added minerals. However, we were unable to determine the species-level changes in the phytoplankton community, and hence whether these trace metals, individually or combined, could account for the observed phytoplankton community photosynthetic performance.

4.2.2. OAE impacts on the zooplankton community

Slag-based OAE did not significantly influence the zooplankton community composition while olivine-based OAE induced some statistically significant effects, including a lower Shannon diversity. The increase in *N. scintillans* abundance and the decrease in *Penilia* sp. and *Oikopleura* sp. in the olivine treatment indicate that the zooplankton response to OAE can vary among different zooplankton types.

The observed lower abundance of *Oikopleura* sp. on day 13 in the olivine treatment may indicate a temporary suppression or a slower growth rate of this zooplankton species in response to the olivine addition. This could be attributed to the potential effects of olivine on the availability of essential nutrients or changes in the physicochemical environment of the water. However, the subsequent increase in *Oikopleura* sp. abundance by day 22 suggests that the growth of this species may have recovered or accelerated in the olivine treatment, leading to a higher abundance compared to the slag treatment and the control on day 22. As discussed in section 4.2.1, reduced *Oikopleura* sp. abundance was unlikely due to reduced food availability since phytoplankton within the preferred edible size spectrum, such as cyanobacteria and nanoeukaryotes, were even more abundant in the olivine treatment. Instead, we hypothesize it to be an effect of the suspended olivine particles that occurred for approximately the first 5 days of the study that were so plentiful that they turned the enclosed seawater milky and may have clogged the mucous feeding mesh of *Oikopleura* sp. (Lombard et al., 2011).

The abundance of *Penilia* sp. and *Oikopleura* sp. was lower in the olivine treatment than the other two groups throughout the experiment while the abundance of *N. scintillans* was consistently higher. The second bloom of cyanobacteria in olivine is likely to be the results of decreased predators, like *Penilia* sp. and *Oikopleura* sp., although the changes in their abundance were not statistically significant between treatments and the control. We cannot provide a particularly convincing hypothesis about what specifically drove these differences though it is tempting to speculate that suspended particles present at the beginning may have played a role also for those organisms since this was the only apparent systematic difference to the control and slag treatment. The proliferation of *N. scintillans* can be problematic since heterotrophic dinoflagellate blooms can regulate phytoplankton communities, cause toxicity to aquatic fish, and create a hypoxic sub-surface zone (Baliarsingh et al., 2016; Zhang et al., 2020; Al-Azri et al., 2007), although a bloom of *N. scintillans* in southeast Australia only induced ichthyotoxicity when the cell concentration reached 2,000,000 cells L^{-1} (Hallegraeff et al., 2019). For comparison, we observed a maximum of 32 cells L^{-1} in one microcosm replicate of the olivine treatment.

690 In comparison to olivine, steel slag seemed to have less potential to affect zooplankton community composition. The
691 abundance of all groups of phytoplankton, apart from microphytoplankton after day 10, was similar in the slag treatment
692 and the control through the experiment. This is probably because the amount of slag powder added in the treatment was
693 much less than the olivine powder resulting in fewer physical particle perturbations to zooplankton. In addition, the
694 chemistry perturbations such as enhanced alkalinity concentration and various dissolved trace metals, especially Mn, from
695 the slag powder did not seem to have a notable direct influence on zooplankton abundance over the three-week period.
696 Even though we did not observe drastic changes in zooplankton abundance during the experiment, considering there was
697 higher microphytoplankton abundance in the slag treatment after day 10, slag powder may benefit some zooplankton
698 especially those who feed on large phytoplankton on a longer time scale.

699

700 **4.2.3. Dissolved trace metal accumulation in seawater and its environmental implications**

701 The addition of olivine and slag as OAE source minerals released trace metals into the seawater, predominantly Al, Fe, Ni,
702 and Cu (olivine) as well as Al, Fe, and Mn (slag). The maximum measured concentrations for dissolved Al, Fe, Ni, Cu, and
703 Mn were 1093, 253, 77, 27, and 810 nmol L^{-1}, respectively. The threshold values for drinking water with health or aesthetic
704 considerations by the Australian Drinking Water Guidelines for Al, Fe, Ni, Cu, and Mn are 7400, 5360, 340, 15600, and
705 1800 nmol L^{-1}, respectively (NRMMC, 2022). All dissolved trace metal concentrations measured herein are well below
706 these health and aesthetic threshold values. In natural freshwater sources, the concentrations of Al, Fe, Ni, Cu and Mn are
707 generally less than 44000, 71400, 510, 156, and 25400 nmol L^{-1} (NRMMC, 2022). Although these natural water data were
708 primarily derived from rivers and streams, they serve as valuable references for evaluating trace metal release in our
709 experiment. Thus, mineral additions to the microcosms as simulated here did not increase thresholds for any of the
710 measured trace metals beyond those that are considered safe for drinking water quality, and they were within the trace
711 metal concentration range in natural water. However, while these guidelines on drinking water provide a good starting point
712 on how to quantify what OAE perturbation could be considered "safe" and "unsafe" with regards to trace metals, it must
713 be recognized that seawater is not drinking water and that critical thresholds may be different in the latter.

714

715 The release of trace metals from OAE materials is considered to have relatively strong effects on biology, particularly in
716 the open ocean where trace metals usually occur in lower concentrations. For example, oceanic Al, Fe, Ni, and Mn
717 concentrations are about 2, 0.5, 8, and 0.3 nmol L^{-1} (Bruland and Lohan, 2003; Sohrin and Bruland, 2011). Previous
718 research on OAE-associated trace metal impacts on individual phytoplankton species grown in laboratory environments
719 has shown that concentration thresholds beyond which trace metal induces negative effects on fitness likely differ between
720 species (Guo et al., 2022; Hutchins et al., 2023; Xin et al., 2023). Indeed, our experiment with plankton communities
721 provides further support that several components of the planktonic food web are affected by OAE. However, our experiment
722 does not allow determining whether observed effects were primarily invoked by carbonate chemistry, macronutrient (P and
723 Si), or trace metal perturbations. Thus, dedicated experiments isolating the impact of these factors on plankton will be
724 required in the future.

725 **4.2.4. Particulate trace metal accumulation in seawater and its environmental implications**

726 The Derwent Estuary (where we collected our plankton communities) was highly metal polluted due to industrial practice
727 (Macleod and Coughanowr, 2019). Both our dissolved and particulate trace metal data indicated high background metal

concentrations, especially for Fe and Zn. Furthermore, the metal:POC ratios found here are higher than reported for open ocean studies or lab cultures. For example, the Fe:POC can vary from 2-136 μmol mol^{-1} depending on the cultured phytoplankton species and the environmental dissolved Fe concentration (Kulkarni et al., 2006; Sunda and Huntsman, 1995; King et al., 2012; Boyd et al., 2015). In our results the Fe:POC values ranged from 1200 to 39 000 μmol mol^{-1}, which may be due to the particulate trace metal richness of the Derwent Estuary (control) and/or the addition of lithogenic particles (slag and olivine treatment). The presence of abiotic particulate metal sources creates challenges to quantify metal quotas and then to evaluate metal accumulation effects on biological organisms.

Our study reveals that the added minerals enriched the particulate trace metal pools to various degrees. Consistent with the dissolved trace metal data, the slag treatment was enriched with particulate Fe and Mn while the olivine treatment was enriched with particulate Fe and Ni. The enhanced particulate Ni and Mn concentrations were higher than before mineral additions and the control levels. This is in line with previous research which indicates a positive correlation between particulate and dissolved trace metal concentrations (Gaulier et al., 2019).

Based on the amounts released through OAE as simulated herein, it appears that Ni and Mn have the highest potential to cause toxicity in certain marine organisms (Jakimska et al., 2011). These trace metals have the potential to accumulate in marine organisms over time (bioaccumulation effects), and their increased concentrations in the food chain can lead to adverse effects on the health and well-being of organisms at higher trophic levels (biomagnification effects). One crucial next step will be to investigate whether the enhanced dissolved/particulate trace metal will affect higher trophic levels to estimate the environmental risks of OAE on other marine organisms.

5 Conclusions

Our study aimed to assess the environmental impacts of two ground OAE minerals, olivine and steel slag, on coastal plankton communities. Both minerals released alkalinity, leading to an elevation in pH_T. However, the addition of steel slag exhibited significantly higher efficiency in elevating alkalinity compared to olivine.

Approximately 1.9 g L^{-1} of olivine powder were added in the olivine treatments, leading to a 29 μmol kg^{-1} increase in alkalinity and increased concentrations of Si(OH)$_4$ and trace metals (Fe and Ni). Compared to this relatively modest increase of alkalinity and associated CO_2 removal potential, the impacts on the plankton community appeared to be relatively pronounced. Thus, although our experiment ran for only 3 weeks, and olivine powder may slowly release more alkalinity, the short-term response monitored here suggests that the immediate climatic benefit is relatively small compared to a relatively pronounced environmental effect.

Only 0.038 g L^{-1} of slag were added to the treatment but this led to an alkalinity enhancement of 361 μmol kg^{-1} and the increased concentrations of macronutrients (P and Si) and trace metals (Mn and Fe) additions as well as changes in carbonate chemistry. Although limited environmental impacts were observed from the slag treatment in our experiment, some aspects require further study. For example, the pronounced release of P could cause eutrophication and the relatively rapid increase in pH may be a detrimental aspect if organisms cannot acclimate fast enough. Furthermore, it is essential to

consider that the composition of steel slag can vary depending on the source factory (Wang et al., 2011; Proctor et al., 2000), which may affect the efficiency of carbon removal and change the trace metal perturbation. Nevertheless, just based on our experiment, the comparison between the immediate climatic benefit and environmental effect appears to be more favourable for slag than olivine.

Based on our findings, it can be concluded that steel slag powder exhibited fewer environmental impacts on plankton communities compared to olivine powder relative to its capacity for alkalinity enhancement. The results highlight the importance of carefully assessing the environmental consequences of using specific OAE minerals, particularly when considering their potential effects on plankton communities.

Data availability. Data are available in the Institute for Marine and Antarctic Studies (IMAS) data catalogue, University of Tasmania (UTAS) (https://doi.org/10.25959/X6FH-9K15, Guo, J., & Bach, L. (2023).).

Author contributions. LTB, RFS, KMS and JAG designed the experiments and JAG carried them out. LTB, RFS and KMS supervised the study. ATT analysed the dissolved/particulate trace metal samples. JAG conducted statistical analyses. JAG prepared the manuscript with contributions from all authors.

Competing interests. The contact author has declared that none of the authors has any competing interests.

Disclaimer. Publisher's note: Copernicus Publications remains neutral with regard to jurisdictional claims in published maps and institutional affiliations.

Acknowledgements. We would like to thank Steve Van Orsouw from Moyne Shire Council, Victoria, Australia for providing olivine rocks. We also thank Bradley Mansell who provided the Basic Oxygen Slag from Liberty Primary Steel Whyalla Steelworks in Whyalla, South Australia, Australia. We thank Sandrin Feig and Thomas Rodemann for their support on scanning electron microscopy and particulate organic matter. We appreciate the assistance of Pam Quayle and Axel Durand (IMAS) in the lab, particularly with particulate metal digestions.

Financial support. This research has been supported by the Australian Research Council through a Future Fellowship project (FT200100846 to LTB), the Carbon to Sea Initiative (LTB), and by the Australian Antarctic Program Partnership (ASCI000002 to RFS, KMS and JAG). Access to SF-ICP-MS instrumentation was facilitated through ARC LIEF funding (LE0989539) awarded to ATT. JAG thanks the Australian Research Training Program (RTP) for her scholarship.

References

Ackerman, L., Jelínek, E., Medaris, G., Ježek, J., Siebel, W., and Strnad, L.: Geochemistry of Fe-rich peridotites and associated pyroxenites from Horní Bory, Bohemian Massif: Insights into subduction-related melt–rock reactions, Chem. Geol., 259, 152-167, https://doi.org/10.1016/j.chemgeo.2008.10.042, 2009.

Al-Azri, A., Al-Hashmi, K., Goes, J., Gomes, H., Rushdi, A. I., Al-Habsi, H., Al-Khusaibi, S., Al-Kindi, R., and Al-Azri, N.: Seasonality of the bloom-forming heterotrophic dinoflagellate Noctiluca scintillans in the Gulf of Oman in relation to environmental conditions, Int. J. Oceans Oceanogr., 2, 51-60, 2007.

Armstrong, F. A.: Why did nature choose manganese to make oxygen?, Philos Trans R Soc Lond B Biol Sci, 363, 1263-1270,

806   https://doi.org/10.1098/rstb.2007.2223, 2008.

807 Bach, L. T., Gill, S. J., Rickaby, R. E. M., Gore, S., and Renforth, P.: CO2 removal with enhanced weathering and ocean
808   alkalinity enhancement: potential risks and co-benefits for marine pelagic ecosystems, Front Clim, 1, 1-21,
809   http://doi.org/10.3389/fclim.2019.00007, 2019.

810 Balaguer, J., Koch, F., Hassler, C. et al.: Iron and manganese co-limit the growth of two phytoplankton groups dominant at
811   two locations of the Drake Passage. Commun Biol 5, 207, https://doi.org/10.1038/s42003-022-03148-8, 2022.

812 Baliarsingh, S. K., Lotliker, A. A., Trainer, V. L., Wells, M. L., Parida, C., Sahu, B. K., Srichandan, S., Sahoo, S., Sahu, K. C., and
813   Kumar, T. S.: Environmental dynamics of red Noctiluca scintillans bloom in tropical coastal waters, Mar. Pollut. Bull.,
814   111, 277-286, https://doi.org/10.1016/j.marpolbul.2016.06.103, 2016.

815 Basu, S. and Mackey, K. R. M.: Phytoplankton as key mediators of the biological carbon pump: their responses to a
816   changing climate, Sustainability, 10, 869, https://doi.org/10.3390/su10030869, 2018.

817 Behrenfeld, M. J., Worthington, K., Sherrell, R. M., Chavez, F. P., Strutton, P., McPhaden, M., and Shea, D. M.: Controls on
818   tropical Pacific Ocean productivity revealed through nutrient stress diagnostics, Nature, 442, 1025-1028,
819   https://doi.org/10.1038/nature05083, 2006.

820 Bowie, A. R., Townsend, A. T., Lannuzel, D., Remenyi, T. A., and van der Merwe, P.: Modern sampling and analytical
821   methods for the determination of trace elements in marine particulate material using magnetic sector inductively
822   coupled plasma-mass spectrometry, Anal Chim Acta, 676, 15-27, https://doi.org/10.1016/j.aca.2010.07.037, 2010.

823 Boyd, P. W., Strzepek, R. F., Ellwood, M. J., Hutchins, D. A., Nodder, S. D., Twining, B. S., and Wilhelm, S. W.: Why are biotic
824   iron pools uniform across high- and low-iron pelagic ecosystems?, Global Biogeochem. Cycles, 29, 1028-1043,
825   http://doi.org/10.1002/2014gb005014, 2015.

826 Boyd, P. W., Jickells, T., Law, C., Blain, S., Boyle, E., Buesseler, K., Coale, K., Cullen, J., De Baar, H. J., and Follows, M.:
827   Mesoscale iron enrichment experiments 1993-2005: synthesis and future directions, Science, 315, 612-617,
828   http://doi.org/10.1126/science.1131669, 2007.

829 Bruland, K. W. and Lohan, M. C.: 6.02 Controls of Trace Metals in Seawater, in: Treatise on Geochemistry, edited by:
830   Elderfield, H., Holland, H. D., and Turekian, K. K., Elsevier Pergamon, 23-47, http://doi.org/10.1016/b0-08-043751-
831   6/06105-3, 2003.

832 Burt, D. J., Fröb, F., and Ilyina, T.: The sensitivity of the marine carbonate system to regional ocean alkalinity enhancement,
833   Front Clim, 3, http://doi.org/10.3389/fclim.2021.624075, 2021.

834 Caserini, S., Storni, N., and Grosso, M.: The availability of limestone and other raw materials for ocean alkalinity
835   enhancement, Global Biogeochem. Cycles, 36, http://doi.org/10.1029/2021gb007246, 2022.

836 De Baar, H. J., Boyd, P. W., Coale, K. H., Landry, M. R., Tsuda, A., Assmy, P., Bakker, D. C., Bozec, Y., Barber, R. T., and Brzezinski,
837   M. A.: Synthesis of iron fertilization experiments: from the iron age in the age of enlightenment, J Geophys Res
838   Oceans, 110, https://doi.org/10.1029/2004JC002601, 2005.

839 Dickson, A. G., Sabine, C. L., and Christian, J. R.: Guide to best practices for ocean CO2 measurements, North Pacific Marine
840   Science Organization, Canada2007.

841 Egge, J. and Jacobsen, A.: Influence of silicate on particulate carbon production in phytoplankton, Mar. Ecol. Prog. Ser.,
842   147, 219-230, http://doi.org/10.3354/meps147219, 1997.

843 Evans, C., O'Reilly, J. E., and Thomas, J.: A handbook for the measurement of chlorophyll and primary production, 1987.

844 Falkowski, P. G.: The role of phytoplankton photosynthesis in global biogeochemical cycles, Photosynthesis Research, 39,
845   235-258, https://doi.org/10.1007/BF00014586, 1994.

846 Feng, E. Y., Koeve, W., Keller, D. P., and Oschlies, A.: Model-based assessment of the CO2 sequestration potential of coastal
847   ocean alkalinization, Earth's Future, 5, 1252-1266, http://doi.org/10.1002/2017ef000659, 2017.

848 Ferderer, A., Chase, Z., Kennedy, F., Schulz, K. G., and Bach, L. T.: Assessing the influence of ocean alkalinity enhancement
849   on a coastal phytoplankton community, Biogeosciences, 19, 5375-5399, http://doi.org/10.5194/bg-19-5375-2022,
850   2022.

851 Ferderer, A., Schulz, K. G., Riebesell, U., Baker, K. G., Chase, Z., and Bach, L. T.: Investigating the effect of silicate and calcium
852   based ocean alkalinity enhancement on diatom silicification, Biogeosciences Discuss. [preprint],
853   https://doi.org/10.5194/bg-2023-144, in review, 2023.

854 Package 'seacarb'-Seawater Carbonate Chemistry: https://cran.r-project.org/web/packages/seacarb/index.html, last
855   access: 2023/6/1.

856 Gaulier, C., Zhou, C., Guo, W., Bratkic, A., Superville, P. J., Billon, G., Baeyens, W., and Gao, Y.: Trace metal speciation in
857   North Sea coastal waters, Sci. Total Environ., 692, 701-712, http://doi.org/10.1016/j.scitotenv.2019.07.314, 2019.

858 Guo, J., Bao, Y., and Wang, M.: Steel slag in China: Treatment, recycling, and management, Waste Management, 78, 318-
859   330, https://doi.org/10.1016/j.wasman.2018.04.045, 2018.

860 Guo, J. A., Strzepek, R., Willis, A., Ferderer, A., and Bach, L. T.: Investigating the effect of nickel concentration on
861   phytoplankton growth to assess potential side-effects of ocean alkalinity enhancement, Biogeosciences, 19, 3683-
862   3697, https://doi.org/10.5194/bg-19-3683-2022, 2022.

Hallegraeff, G. M., Albinsson, M. E., Dowdney, J., Holmes, A. K., Mansour, M. P., and Seger, A.: Prey preference, environmental tolerances and ichthyotoxicity by the red-tide dinoflagellate Noctiluca scintillans cultured from Tasmanian waters, J. Plankton Res., 41, 407-418, https://doi.org/10.1093/plankt/fbz037, 2019.

Hansen, H. P. and Koroleff, F.: Determination of nutrients, in: Methods of seawater analysis, edited by: Grasshoff, K., Kremling, K., and Ehrhardt, M., 159-228, https://doi.org/10.1002/9783527613984.ch10, 1999.

Hartmann, J., West, A. J., Renforth, P., Köhler, P., De La Rocha, C. L., Wolf-Gladrow, D. A., Dürr, H. H., and Scheffran, J.: Enhanced chemical weathering as a geoengineering strategy to reduce atmospheric carbon dioxide, supply nutrients, and mitigate ocean acidification, Rev. Geophys., 51, 113-149, http://doi.org/10.1002/rog.20004, 2013.

Humphreys, M. P., Lewis, E. R., Sharp, J. D., and Pierrot, D.: PyCO2SYS v1. 8: marine carbonate system calculations in Python, Geosci Model Dev, 15, 15-43, https://doi.org/10.5194/gmd-15-15-2022, 2022.

Hutchins, D. A., Fu, F.-X., Yang, S.-C., John, S. G., Romaniello, S. J., Andrews, M. G., and Walworth, N. G.: Responses of globally important phytoplankton species to olivine dissolution products and implications for carbon dioxide removal via ocean alkalinity enhancement, Biogeosciences, 20, 4669–4682, https://doi.org/10.5194/bg-20-4669-2023, 2023.

Ilyina, T., Wolf‐Gladrow, D., Munhoven, G., and Heinze, C.: Assessing the potential of calcium‐based artificial ocean alkalinization to mitigate rising atmospheric CO2 and ocean acidification, Geophys. Res. Lett., 40, 5909-5914, https://doi.org/10.1002/2013GL057981, 2013.

Jakimska, A., Konieczka, P., Skóra, K., and Namieśnik, J.: Bioaccumulation of metals in tissues of marine animals, Part II: metal concentrations in animal tissues, Pol J Environ Stud, 20, 2011.

Keller, D. P., Feng, E. Y., and Oschlies, A.: Potential climate engineering effectiveness and side effects during a high carbon dioxide-emission scenario, Nat. Commun., 5, 3304, https://doi.org/10.1038/ncomms4304, 2014.

King, A. L., Sañudo-Wilhelmy, S. A., Boyd, P. W., Twining, B. S., Wilhelm, S. W., Breene, C., Ellwood, M. J., and Hutchins, D. A.: A comparison of biogenic iron quotas during a diatom spring bloom using multiple approaches, Biogeosciences, 9, 667-687, http://doi.org/10.5194/bg-9-667-2012, 2012.

Kohler, P., Hartmann, J., and Wolf-Gladrow, D. A.: Geoengineering potential of artificially enhanced silicate weathering of olivine, Proc. Natl. Acad. Sci. USA, 107, 20228-20233, https://doi.org/10.1073/pnas.1000545107, 2010.

Kourounis, S., Tsivilis, S., Tsakiridis, P. E., Papadimitriou, G. D., and Tsibouki, Z.: Properties and hydration of blended cements with steelmaking slag, Cem. Concr. Res., 37, 815-822, https://doi.org/10.1016/j.cemconres.2007.03.008, 2007.

Kulkarni, P. P., She, Y. M., Smith, S. D., Roberts, E. A., and Sarkar, B.: Proteomics of metal transport and metal-associated diseases, Chemistry, 12, 2410-2422, http://doi.org/10.1002/chem.200500664, 2006.

Lenton, A., Matear, R. J., Keller, D. P., Scott, V., and Vaughan, N. E.: Assessing carbon dioxide removal through global and regional ocean alkalinization under high and low emission pathways, Earth. Syst. Dyn., 9, 339-357, https://doi.org/10.5194/esd-9-339-2018, 2018.

Lombard, F., Selander, E., and Kiørboe, T.: Active prey rejection in the filter-feeding appendicularian Oikopleura dioica, Limnol. Oceanogr., 56, 1504-1512, http://doi.org/10.4319/lo.2011.56.4.1504, 2011.

Lueker, T. J., Dickson, A. G., and Keeling, C. D.: Ocean pCO2 calculated from dissolved inorganic carbon, alkalinity, and equations for K1 and K2: validation based on laboratory measurements of CO2 in gas and seawater at equilibrium, Mar. Chem., 70, 105-119, https://doi.org/10.1016/S0304-4203(00)00022-0, 2000.

Macleod, C. and Coughanowr, C.: Heavy metal pollution in the Derwent estuary: History, science and management, Reg. Stud. Mar. Sci., 32, http://doi.org/10.1016/j.rsma.2019.100866, 2019.

Moore, C. M., Mills, M. M., Arrigo, K. R., Berman-Frank, I., Bopp, L., Boyd, P. W., Galbraith, E. D., Geider, R. J., Guieu, C., Jaccard, S. L., Jickells, T. D., La Roche, J., Lenton, T. M., Mahowald, N. M., Marañón, E., Marinov, I., Moore, J. K., Nakatsuka, T., Oschlies, A., Saito, M. A., Thingstad, T. F., Tsuda, A., and Ulloa, O.: Processes and patterns of oceanic nutrient limitation, Nat. Geosci., 6, 701-710, http://doi.org/10.1038/ngeo1765, 2013.

Nelson, D. M., Smith Jr, W. O., Muench, R. D., Gordon, L. I., Sullivan, C. W., and Husby, D. M.: Particulate matter and nutrient distributions in the ice-edge zone of the Weddell Sea: relationship to hydrography during late summer, Deep. Sea. Res. A, 36, 191-209, https://doi.org/10.1016/0198-0149(89)90133-7, 1989.

NRMMC, N. a.: The Australian Drinking Water Guidelines (2011) - Version 3.8 Updated 2022, 2022.

Pausch, F., Bischof, K., Trimborn, S.: Iron and manganese co-limit growth of the Southern Ocean diatom *Chaetoceros debilis*. PLOS ONE 14, e0221959.. https://doi.org/10.1371/journal.pone.0221959, 2019.

Paquay, F. S. and Zeebe, R. E.: Assessing possible consequences of ocean liming on ocean pH, atmospheric CO2 concentration and associated costs, Int. J. Greenh. Gas Control., 17, 183-188, https://doi.org/10.1016/j.ijggc.2013.05.005, 2013.

Platt, T., Gallegos, C. L., and Harrison, W. G.: Photoinhibition of photosynthesis in natural assemblages of marine phytoplankton, J. Mar. Res., 38, 687-701, 1980.

Proctor, D. M., Fehling, K. A., Shay, E. C., Wittenborn, J. L., Green, J. J., Avent, C., Bigham, R. D., Connolly, M., Lee, B.,

920   Shepker, T. O., and Zak, M. A.: Physical and chemical characteristics of blast furnace, basic oxygen furnace, and
921   electric arc furnace steel industry slags, Environ. Sci. Technol., 34, 1576-1582, http://doi.org/10.1021/es9906002,
922   2000.

923   Reichl, C., Schatz, M., and Zsak, G.: World mining data, 1-261, 2018.

924   Renforth, P.: The negative emission potential of alkaline materials, Nat. Commun., 10, http://doi.org/10.1038/s41467-
925   019-09475-5, 2019.

926   Renforth, P. and Henderson, G.: Assessing ocean alkalinity for carbon sequestration, Rev. Geophys., 55, 636-674,
927   http://doi.org/10.1002/2016rg000533, 2017.

928   Schallenberg, C., Strzepek, R. F., Schuback, N., Clementson, L. A., Boyd, P. W., and Trull, T. W.: Diel quenching of Southern
929   Ocean phytoplankton fluorescence is related to iron limitation, Biogeosciences, 17, 793-812,
930   https://doi.org/10.5194/bg-17-793-2020, 2020.

931   Schuiling, R. D. and Krijgsman, P.: Enhanced weathering: an effective and cheap tool to sequester CO2, Clim. Change, 74,
932   349-354, https://doi.org/10.1007/s10584-005-3485-y, 2006.

933   Selfe, C.: Developing Transfer Function to Measuring Phytoplankton Cellular Properties with Flow Cytometry, Master's
934   thesis, Institute of Marine and Antarctic Studies, University of Tasmania, Australia, 2022.

935   Comparing smooths in factor-smooth interactions II ordered factors:
936   https://fromthebottomoftheheap.net/2017/12/14/difference-splines-ii/, last access: March 2023.

937   Smith, S. M., Geden, O., Nemet, G. F., Gidden, M. J., Lamb, W. F., Powis, C., Bellamy, R., Callaghan, M. W., Cowie, A., Cox,
938   E., Fuss, S., Gasser, T., Grassi, G., Greene, J., Lück, S., Mohan, A., Müller-Hansen, F., Peters, G. P., Pratama, Y., Repke,
939   T., Riahi, K., Schenuit, F., Steinhauser, J., Strefler, J., Valenzuela, J. M., and Minx, J. C.: The State of Carbon Dioxide
940   Removal - 1st Edition, http://doi.org/10.17605/OSF.IO/W3B4Z, 2023.

941   Sohrin, Y. and Bruland, K. W.: Global status of trace elements in the ocean, TrAC, Trends Anal. Chem., 30, 1291-1307,
942   https://doi.org/10.1016/j.trac.2011.03.006, 2011.

943   Strzepek, R. F. and Harrison, P. J.: Photosynthetic architecture differs in coastal and oceanic diatoms, Nature, 431, 689-
944   692, http://doi.org/10.1038/nature02954, 2004.

945   Su, B., Chen, Y., Guo, S., and Liu, J.: Origins of orogenic dunites: petrology, geochemistry, and implications, Gondwana Res.,
946   29, 41-59, https://doi.org/10.1016/j.gr.2015.08.001, 2016.

947   Subhas, A. V., Marx, L., Reynolds, S., Flohr, A., Mawji, E. W., Brown, P. J., and Cael, B.: Microbial ecosystem responses to
948   alkalinity enhancement in the North Atlantic Subtropical Gyre, Front Clim, 4,
949   https://doi.org/10.3389/fclim.2022.784997, 2022.

950   Sunda, W. G.: Trace metal–phytoplankton interactions in aquatic systems, in: Environmental Microbe–Metal Interactions,
951   edited by: Lovley, D. R., 79-107, https://doi.org/10.1128/9781555818098.ch4, 2000.

952   Sunda, W. G.: Feedback interactions between trace metal nutrients and phytoplankton in the ocean, Frontiers in
953   Microbiology, 3, 1-22, http://doi.org/10.3389/fmicb.2012.00204, 2012.

954   Sunda, W. G. and Huntsman, S. A.: Iron Uptake and Growth Limitation in Oceanic and Coastal Phytoplankton, Marine
955   Chemistry, 50, 189-206, Doi 10.1016/0304-4203(95)00035-P, 1995.

956   Sunda, W. G. and Huntsman, S. A.: Interrelated influence of iron, light and cell size on marine phytoplankton growth,
957   Nature, 390, 389-392, http://doi.org/10.1038/37093, 1997.

958   Tang, D. G. and Morel, F. M. M.: Distinguishing between cellular and Fe-oxide-associated trace elements in phytoplankton,
959   Mar. Chem., 98, 18-30, http://doi.org/10.1016/j.marchem.2005.06.003, 2006.

960   Tovar-Sanchez, A., Sanudo-Wilhelmy, S. A., Garcia-Vargas M., Weaver R. S., Popels L., C., and Hutchins D. A.: A trace metal
961   clean reagent to remove surface-bound iron from marine phytoplankton. Mar. Chem., 82, 1-2, 91-99,
962   https://doi.org/10.1016/S0304-4203(03)00054-9, 2003.

963   Twining, B. S. and Baines, S. B.: The trace metal composition of marine phytoplankton, Ann. Rev. Mar. Sci., 5, 191-215,
964   http://doi.org/10.1146/annurev-marine-121211-172322, 2013.

965   Wafar, M., Le Corre, P., and L'Helguen, S.: ƒ-Ratios calculated with and without urea uptake in nitrogen uptake by
966   phytoplankton, Deep Sea Res. I Oceanogr. Res. Pap., 42, 1669-1674, https://doi.org/10.1016/0967-
967   0637(95)00066-F, 1995.

968   Wang, Q., Yan, P., and Feng, J.: A discussion on improving hydration activity of steel slag by altering its mineral
969   compositions, J. Hazard. Mater., 186, 1070-1075, https://doi.org/10.1016/j.jhazmat.2010.11.109, 2011.

970   Wang, W.: Interactions of trace metals and different marine food chains, Mar. Ecol. Prog. Ser., 243, 295-309,
971   http://doi.org/10.3354/meps243295, 2002.

972   Wolfe-Simon, F., Grzebyk, D., Schofield, O., and Falkowski, P. G.: The role and evolution of superoxide dismutases in algae,
973   J. Phycol., 41, 453-465, https://doi.org/10.1111/j.1529-8817.2005.00086.x, 2005.

974   Xin, X., Faucher, G., and Riebesell, U.: Phytoplankton response to Increased nickel in the context of ocean alkalinity
975   enhancement, Biogeosciences [preprint], https://doi.org/10.5194/bg-2023-130, 2023.

976   Zhang, W., Dong, Z., Zhang, C., Sun, X., Hou, C., Liu, Y., Wang, L., Ma, Y., and Zhao, J.: Effects of physical-biochemical

977   coupling processes on the Noctiluca scintillans and Mesodinium red tides in October 2019 in the Yantai nearshore,
978   China, Mar. Pollut. Bull., 160, 111609, https://doi.org/10.1016/j.marpolbul.2020.111609, 2020.
979